iScience

CellPress
OPEN ACCESS

Article

Chemogenetic activation of astrocytes promotes remyelination and restores cognitive deficits in visceral hypersensitive rats

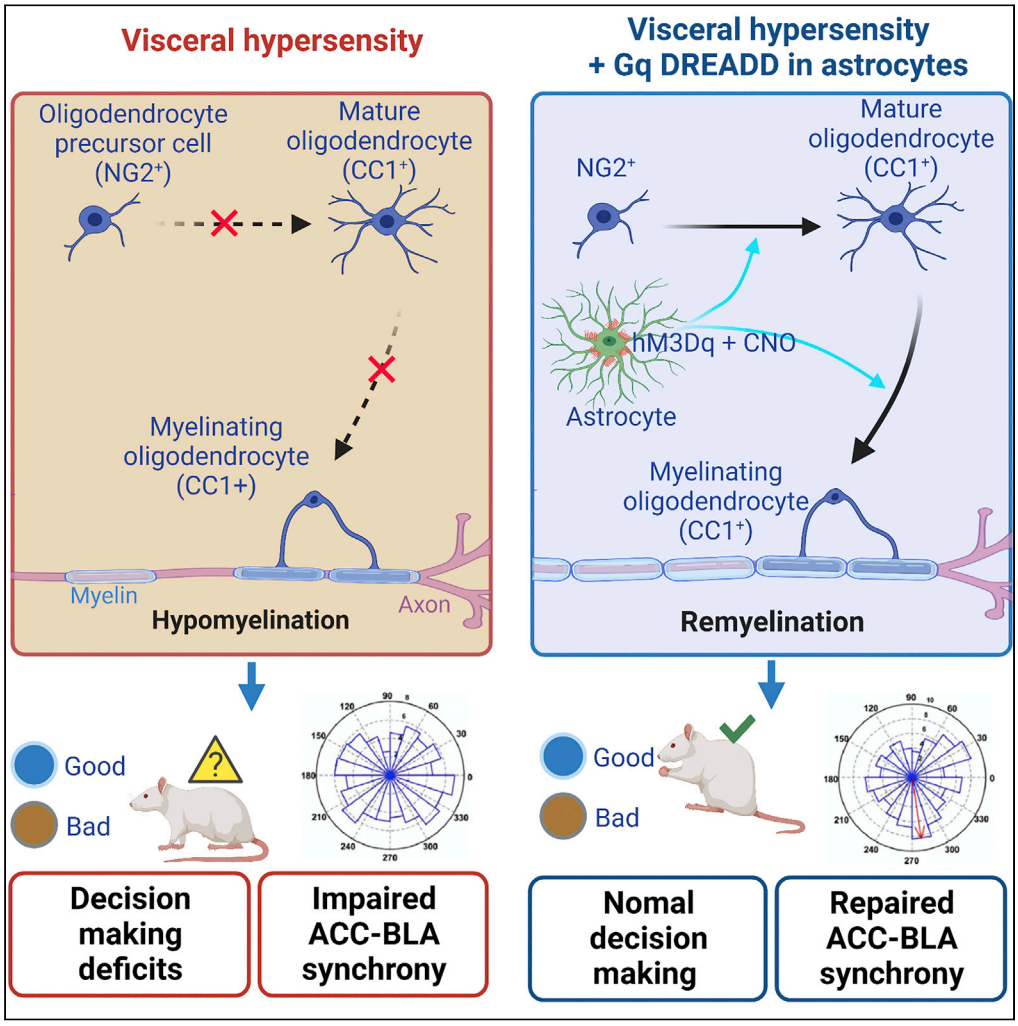

Mahadi Hasan, Zhuogui Lei, Mastura Akter, Zafar Iqbal, Faeeqa Usaila, Aruna Surendran Ramkrishnan, Ying Li

yingli@cityu.edu.hk

Highlights

Visceral hypersensitivity causes hypomyelination and suppresses oligodendrogenesis

Chemogenetic activation of astrocytes promotes oligodendrogenesis and remyelination

Chemogenetic activation of astrocytes rescues decision making deficits in VH rats

Chemogenetic activation of astrocytes repairs VH induced desynchronization

Hasan et al., iScience 26, 105840
January 20, 2023
https://doi.org/10.1016/j.isci.2022.105840

iScience

CellPress
OPEN ACCESS

Article

Chemogenetic activation of astrocytes promotes remyelination and restores cognitive deficits in visceral hypersensitive rats

Mahadi Hasan,[1,2,5] Zhuogui Lei,[1,2,3,5] Mastura Akter,[1,2] Zafar Iqbal,[1,2,3] Faeeqa Usaila,[1,2] Aruna Surendran Ramkrishnan,[1,2] and Ying Li[1,2,3,4,6,*]

SUMMARY

Using a well-established chronic visceral hypersensitivity (VH) rat model, we characterized the decrease of myelin basic protein, reduced number of mature oligodendrocytes (OLs), and hypomyelination in the anterior cingulate cortex (ACC). The results of rat gambling test showed impaired decision-making, and the results of electrophysiological studies showed desynchronization in the ACC to basolateral amygdala (BLA) neural circuitry. Astrocytes release various factors that modulate oligodendrocyte progenitor cell proliferation and myelination. Astrocytic Gq-modulation through expression of hM3Dq facilitated oligodendrocyte progenitor cell proliferation and OL differentiation, and enhanced ACC myelination in VH rats. Activating astrocytic Gq rescued impaired decision-making and desynchronization in ACC-BLA. These data indicate that ACC hypomyelination is an important component of impaired decision-making and network desynchronization in VH. Astrocytic Gq activity plays a significant role in oligodendrocyte myelination and decision-making behavior in VH. Insights from these studies have potential for interventions in myelin-related diseases such as chronic pain-associated cognitive disorders.

INTRODUCTION

Myelination of the brain occurs concurrently with cognitive and behavioral development.[1] Various studies have established the dynamic nature of myelin, changes to which contribute greatly to maintaining cognitive function and brain plasticity.[2–5]

In patients with irritable bowel syndrome (IBS),[6] imaging studies have demonstrated the existence of gray matter and white matter abnormalities in the insula, ACC and corpus callosum areas.[7,8] Magnetic resonance imaging (MRI) and diffusion tensor imaging (DTI) studies in patients with IBS have shown that pain severity and pain unpleasantness are correlated with mean fractional anisotropy (FA) extracted from white matter (WM) regions associated with nociception of the anterior insula and thalamus.[6] Impaired myelination has been demonstrated in human subjects with chronic visceral pain. However, *in vivo* evidence of myelin plasticity in the chronic pain state utilizing an animal model is lacking.

Visceral hypersensitivity (VH) is a fundamental neurological and gastrointestinal abnormality observed in IBS patients. We utilized a rat model with colonic anaphylaxis evoked by intraperitoneal injection of chicken egg albumin[9] that has been shown by numerous investigators[10,11] including ourselves,[12–15] to be a suitable model to study post inflammatory conditions of visceral hyperalgesia such as post infection IBS which occurs in up to 20% of patients following acute gastrointestinal infection. The clinical connection between visceral pain and increased incidences of depression, social anxiety, and other cognitive disorders has been well established.[16] Symptoms of major depressive disorder (MDD) occur in 90% of IBS patients.[7] Chronic pain patients perform poorly in gambling-like and reward-related tasks that involve strategic planning and decision-making such as the Iowa Gambling Task.[7,17] Our published data reported that chronic visceral hypersensitivity is associated with decision-making deficits.[18,19] Impaired lactate release from astrocytes disrupted ACC neural activity, causing cognitive dysfunction in the chronic visceral hypersensitivity state.[19] Using a visceral hypersensitivity (VH) rat model, in this study, we examine the impairment of

[1]Department of Neuroscience, City University of Hong Kong, Hong Kong SAR, China

[2]Department of Biomedical Sciences, City University of Hong Kong, Hong Kong SAR, China

[3]Centre for Regenerative Medicine and Health, Hong Kong Institute of Science & Innovation, Chinese Academy of Sciences, Hong Kong SAR, China

[4]Centre for Biosystems, Neuroscience, and Nanotechnology, City University of Hong Kong, Hong Kong SAR, China

[5]These authors contributed equally

[6]Lead contact

*Correspondence: yingli@cityu.edu.hk

https://doi.org/10.1016/j.isci.2022.105840

oligodendrocyte function in the cortex associated with decision-making ability of rats with chronic visceral hypersensitivity.

Chronic pain patients have been reported to have elevated levels of pro-inflammatory cytokines.[20,21] Our previous study showed development of reactive astrogliosis in the chronic VH rat model.[19] The results of a recent study have shown increases in microglial activity and cytokine expression in chronic trigeminal neuropathy.[22] Microglia play a crucial role in neurodevelopment by interacting with neuronal cells such as OLs for wiring and neural circuit regulation.[23] Given that cumulative evidence of elevated levels of pro-inflammatory cytokines, such as IL-1β, IL-6, and TNF-α, have been reported in patients suffering from chronic pain[20,24] and experimental animal models with pain,[17,21] and that oligodendroglia are markedly susceptible to inflammation-induced excitotoxicity in both rodents and humans,[25,26] in this study, we assess cytokines and microglial activity associated with hypomyelination in chronic visceral hypersensitivity rats.

Brain activity is characteristically rhythmic and interactions between various brain regions is essential for complex information processing.[27,28] Myelination accelerates nerve impulse propagation along the axon, facilitating long-range oscillations and synchrony of spike time arrival between neurons in different brain regions.[29,30] Modifications to myelin play a key role in brain plasticity and learning and memory.[2–5,31] Our published data demonstrate that phase-locking and synchronization within the ACC and between the ACC and BLA play a major role in the modulation of decision-making behavior in rats.[18,19] However, the underlying neural network mechanisms are not clear. Active neurons have been shown to modulate myelination.[31,32] Conversely, dysfunctional neuronal circuitry has been identified in chronic visceral hypersensitivity[18,19] and neuropsychiatric disorders.[33,34] Neurological disorders which are conventionally accompanied by neuronal dysfunction may stem from the disruption of myelin plasticity. We tested our hypotheses that hypomyelination is the important mechanism underlying impaired cortical neural network functioning and decision-making in the chronic visceral hypersensitivity state.

It is clear that astrocytes play a crucial role in the modulation of neuronal activity and synaptic plasticity. Astrocytes regulate the release of neurotransmitters, and energy substrates such as lactate,[19,76] which are considered to be involved in learning and memory.[35] Increasing neuronal activity has been shown to enhance the generation of oligodendrocytes and thickness of individual myelin segments.[32] Oligodendrocytes are responsible for remyelination, a process regulated by intrinsic pathways and facilitated by extrinsic factors from surrounding cells. Despite the surging interest in the role of the astrocytes in promoting myelin structure and conduction velocity[29] through their direct involvement on proliferation, differentiation and migration of oligodendrocytes,[36] limited attention has been given to the influence of astrocytic–oligodendrocyte signaling in promoting myelination, facilitating recovery of cognitive performance (decision-making), and modulating ACC neuronal network in chronic pain.

In this study, we use chemogenetic activation of astrocytes to show that astrocytic–oligodendrocyte signaling is responsible for promoting oligodendrogenesis and adaptive myelination and plays a critical role in the modulation of spike timing accuracy of the ACC neuronal network and improving cognitive performances in both normal and chronic visceral hypersensitivity rats.

RESULTS

Chronic visceral hypersensitivity causes ACC and corpus callosum hypomyelination

Although there is evidence of impaired myelination in human subjects with chronic visceral pain[6] and animal models of trigeminal neuropathic pain,[22] animal studies of myelin plasticity in chronic visceral hypersensitivity still lacking. We examined MBP, a biomarker for myelin basic protein, through immunohistochemistry. Quantitative analysis after normalizing with control revealed a lower intensity of MBP^+ fibers in the VH rats than in the controls (Figure 1A). Western blot analyses of MBP extracted from the ACC also revealed a reduction in MBP expression in VH rats (Figure 1B). Ultrastructural analyses performed by electron microscopy (EM) showed that chronic visceral hypersensitivity significantly reduce the density of unmyelinated axons in the ACC of VH rats compare to control (Figures 1C and 1D). Quantitative assessment of the G-ratio of myelinated fibers further revealed that the myelin sheath thickness had been compromised in VH rats (0.692 ± 0.07) compared to the control (0.627 ± 0.07), whereas the thickness of axons had not been altered (Figures 1E and 1F). Furthermore, MBP expression in the corpus callosum

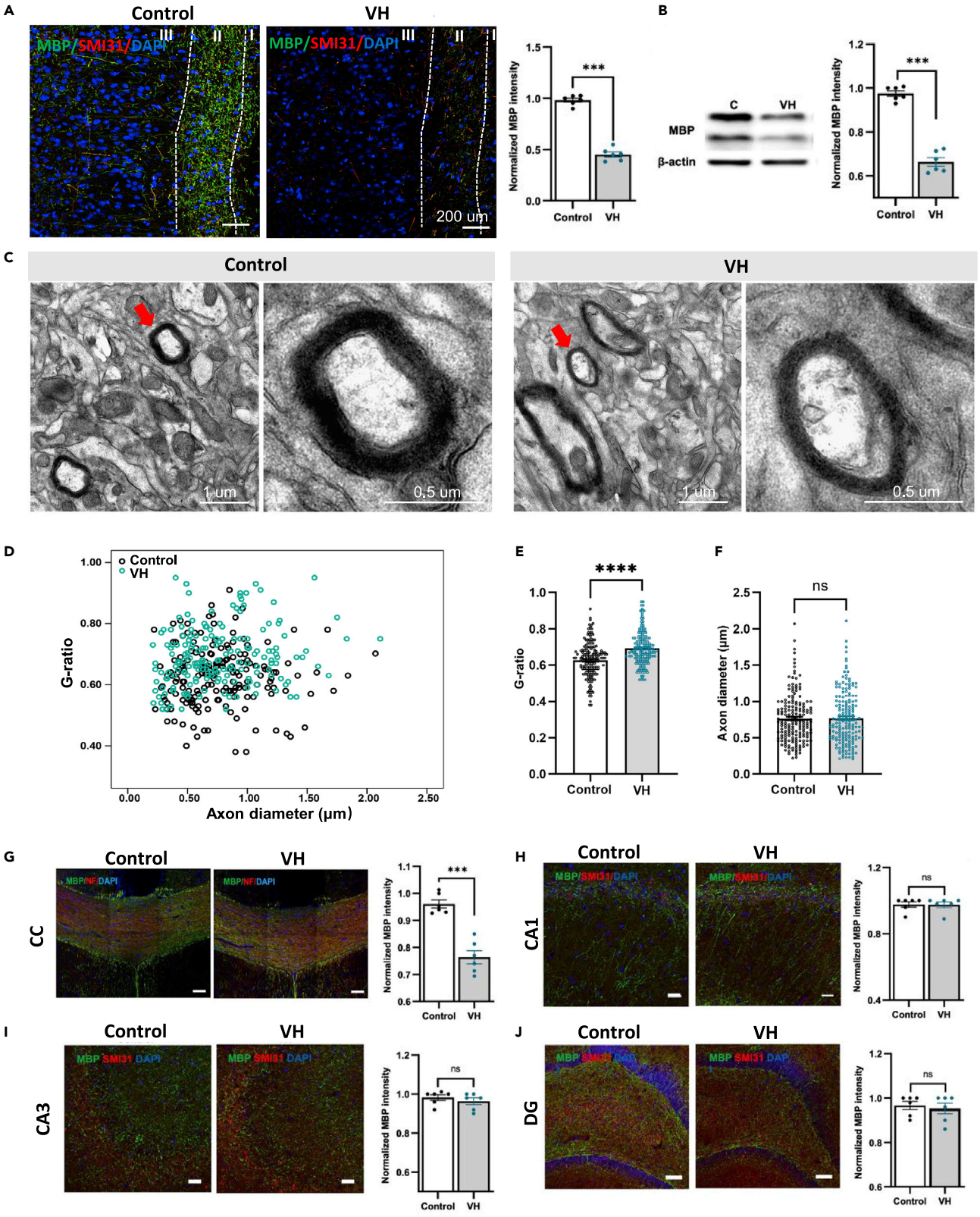
A
Control
VH
MBP/SMI31/DAPI
III
II
I
200 um
Normalized MBP intensity
***
Control
VH
B
C
VH
MBP
β-actin
Normalized MBP intensity
***
Control
VH
C
Control
VH
1 um
0.5 um
D
Control
VH
G-ratio
Axon diameter (μm)
E
****
G-ratio
Control
VH
F
ns
Axon diameter (μm)
Control
VH
G
CC
Control
VH
MBP/NF/DAPI
Normalized MBP intensity
***
Control
VH
H
CA1
Control
VH
MBP/SMI31/DAPI
Normalized MBP intensity
ns
Control
VH
I
CA3
Control
VH
MBP SMI31 DAPI
Normalized MBP intensity
ns
Control
VH
J
DG
Control
VH
MBP SMI31 DAPI
Normalized MBP intensity
ns
Control
VH

Figure 1. Chronic visceral hypersensitivity causes ACC and corpus callosum hypomyelination

(A) Representative confocal images and relative intensity of MBP expression in the ACC region (layer I to IV, sections from 2.2 to 3.8 mm from the bregma) of control and VH rats show decreased MBP expression in VH rats.

(B) Western blotting (WB) of BMP. β-actin, loading control. Mean MBP intensity analysis revealed that VH rats have lower levels of MBP compared to control rats.

(C) Electron micrographs of ACC region showing myelinated axon in control rats and VH rats.

(D) Scatterplot diagram of G-ratios in control rats (blue circle, n = 5 rats) and VH rats (green circle, n = 5 rats per group) showing a smaller number of thin and/or hypomyelinated axons in VH rats.

(E and F) Average G-ratio of myelinated axons in the ACC region in VH and control rats whereas axonal diameters did not change significantly between the two groups.

(G–J) IHC of MBP in the corpus callosum (CC, sections from +0.16 to −1.59 mm AP from the bregma) and different parts of hippocampus (CA1 and CA3; −1.8 to −2.3 mm from bregma; DG;−1.46 to −3.8 mm from bregma) in control and VH rats. Scale bars: (A and H) 100 μm; (C) 1 μm; (I-K) 50 μm.

Data are presented as mean ± SEM (***p < 0.001, ****p < 0.0001 by Unpaired two-tailed Student's *t* test).

was also reduced in the VH rats (Figure 1G, $p < 0.001$), whereas no significant difference was observed in the hippocampus in between groups (Figures 1H–1J).

Chronic visceral hypersensitivity suppressed oligodendrogenesis

Next, we characterize the effects of chronic visceral hypersensitivity on oligodendrocyte progenitor cell (OPC) proliferation and oligodendrocyte (OL) population. We performed immunohistochemistry to determine the absolute number of OPCs ($NG2^+$ cells, a biomarker for OPC cells) and OLs ($CC1^+$ cells, a biomarker for OLs cells) in the ACC (Cg1 and Cg2) of VH and control rats (Figure 2A). We observed an increased number of $NG2^+$ OPCs in VH rats compared to the control (Figures 2B and 2C). In contrast, a significant decrease in the absolute number of $CC1^+$ OLs was detected in VH rats (Figures 2D and 2E). To identify the fate of the OPC proliferation and differentiation into mature OLs, thymidine analog 5-ethynyl-2-deoxyuridine (EdU) was administered to rats through i.p. after the last day of VH induction and the rats were sacrificed 7–10 days later. A significant increase was observed in the fraction of $NG2^+$ OPCs that were EdU labeled ("labeling index") in VH rats relative to the control (Figures 2F and 2G). Furthermore, to clarify whether VH could prevent oligodendrogenesis and limit the formation of mature myelinating OLs, we followed the same protocol and quantified the "labeling index" of $CC1^+$ cells that were labeled with EdU. A significant decrease was observed in the fraction of $CC1^+$ OLs that were EdU labeled in VH rats relative to the control (Figures 2H and 2I). To determine whether the newly formed and reactive OPCs further differentiated to form mature myelinating OLs in VH rats, we conducted immunohistochemistry and western blot to identify the MyRF (a transcription factor necessary for differentiation of immature OLs to mature OLs) expression. We found reduced MyRF expression in the ACC of VH rats compared to the control (Figures 2J–2M), suggesting that visceral hypersensitivity downregulates the MyRF gene, preventing OLs maturation and myelination which ultimately resulted in the hypomyelination of ACC in VH rats.

Visceral hypersensitivity causes ACC neuroinflammation and astrogliosis

The elevated levels of pro-inflammatory cytokines, such as IL-1β, IL-6, and TNF-α, have been reported in patients suffering from chronic pain[20] and animal models of neuropathy pain.[22] To examine the neuroinflammatory reaction in response to chronic visceral hypersensitivity in our VH model, we performed immunohistochemistry to determine the relative expression of inflammatory cells ($CD68^+$ cells, a biomarker for reactive microglia) and inflammatory cytokines (IL1β, a biomarker for inflammatory cytokine, interleukin 1) in the ACC (Figure 3A). A significant increase in the population of ameboid shaped $CD68^+$ cells were observed in the ACC of VH rats, indicating an inflammatory reaction in the ACC of VH rats. In comparison, stellate ramified shaped $CD68^+$ cells were observed in control rats, indicating the presence of resting cells (Figures 3B and 3C). Furthermore, staining and western blot analysis of IL1β revealed higher expression of $IL1\beta^+$ cells in VH rats compared to the control (Figures 3F, 3G, and 3J). We then checked the expression of glial fibrillary acidic protein (GFAP) and S100 calcium-binding protein beta (S100β), markers of astrocytes in VH rats. Immunostaining data and western blot analyses revealed that the density of GFAP+ cells in the ACC was significantly increased in VH rats compared to the controls (Figures 3D, 3E, and 3K). The density of S100β + cells was also increased to 953 in VH rats compared with 484 cells/mm2 in controls (Figures 3H and 3I). All together, these observations indicate the development of ACC neuroinflammation and reactive astrogliosis in the chronic VH rat model.

Impairment of decision-making in visceral hypersensitivity

Pain impairs cognitive performance; to assess decision-making behavior, an executive function, in VH rats, we performed rat gambling task (RGT) (Figure 4). Consistent with our previous publications,[14,19] we found no significant difference in the general activities (Figures 4A and 4B) and three types of decision-making performers

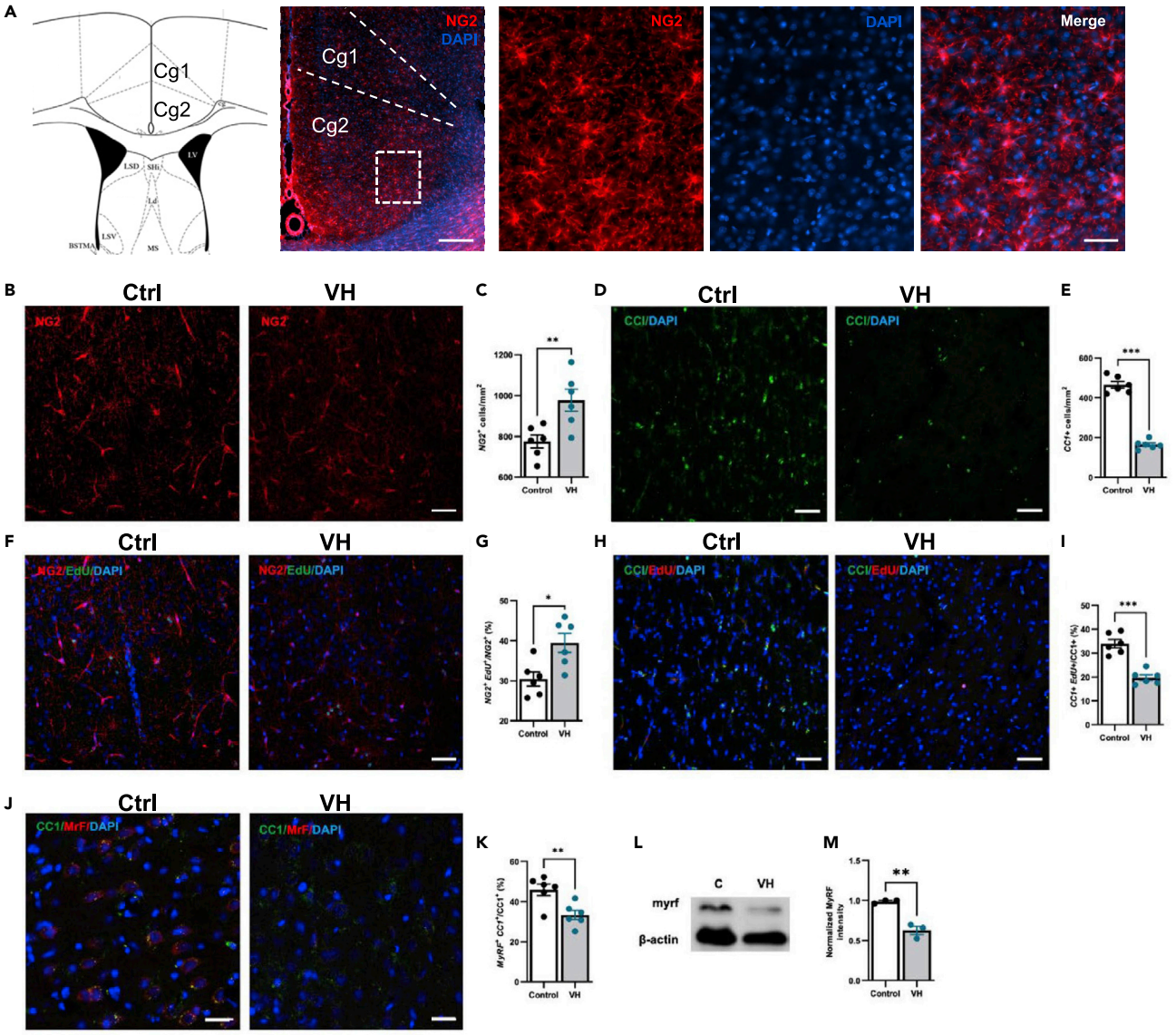

Figure 2. Chronic visceral hypersensitivity suppresses oligodendrogenesis

(A) Schematic figure of ACC (Cg1 and Cg2); representative confocal micrographs NG2$^+$ (red) OPCs in the ACC (Bregma 0.62 mm) with DAPI (blue) (right, higher magnification images).

(B and C) Representative confocal micrographs and quantification of NG2$^+$ (green) OPCs in the ACC of control and VH rats. DAPI (blue) was used as a nuclear counterstain.

(D and E) Representative confocal images and quantification of CC1$^+$ (green) mature oligodendrocytes (OLs) in ACC of control and VH rats.

(F and G) Triple immunohistochemistry (IHC) and quantification of NG2$^+$ (red) and EdU$^+$ (green) OPCs with an overlay of DAPI (blue) in the ACC of control and VH rats.

(H and I) Triple IHC and quantification of CC1$^+$ (green) EdU$^+$ (red) OLs with an overlay of DAPI (blue) in the ACC of control and VH rats.

(J and K) Triple IHC and quantification of CC1$^+$ (green) MyRF$^+$ (red) matured OLs in the ACC of control and VH rats.

(L and M) Western blotting (WB) and analysis of MyRF. β-actin, loading control. Values were normalized with control.

Scale bars: (A left) 250 μm, (A right) 50 μm (B, D, F, and H) 50 μm, (J) 20 μm

Data are presented as mean ± SEM (*p < 0.05, **p < 0.01, ***p < 0.001 by Unpaired two-tailed Student's *t* test).

were identified (Figures 4C–4E). In the VH group, there was a smaller proportion of good decision-makers (35%) compared to the controls (62.7%). (Figures 4C–4E). The difference in proportions of the three behavioral sub-groups (Figure 4F, $p < 0.05$) and total food consumption (Figure 4G) between the control and VH groups were significant, suggesting that chronic visceral hypersensitivity impaired decision-making ability.

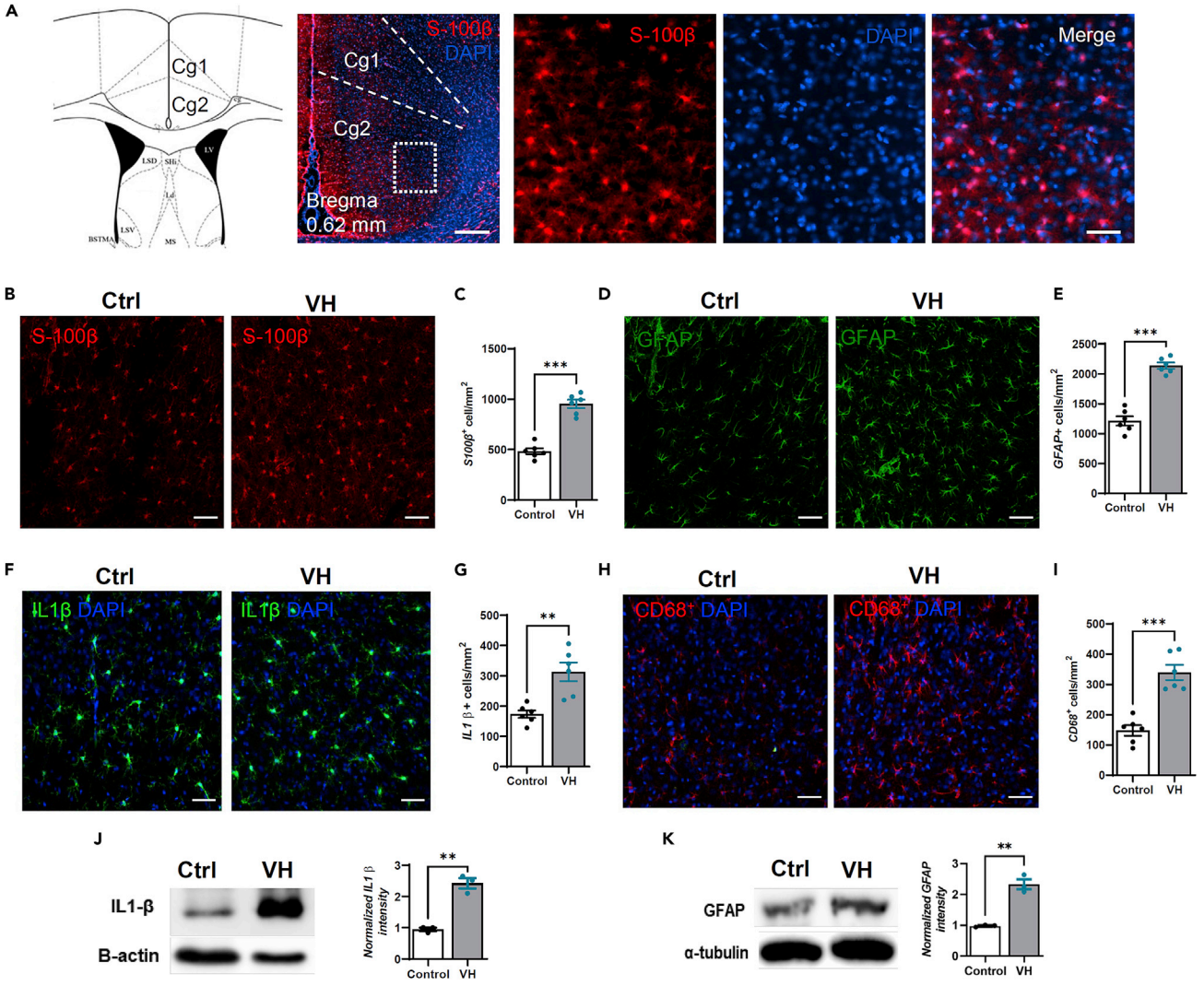

Figure 3. Visceral hypersensitivity causes ACC neuroinflammation and astrogliosis

(A) Schematic figure of ACC (Cg1 and Cg2); representative confocal micrographs S-100β+ (red) astrocytes in the ACC (Bregma 0.62 mm) with DAPI (blue) (right, higher magnification images).

(B and C) Representative confocal images and quantification of CD68 + (red) microglia in ACC of control and VH rats. DAPI (blue) was used as a nuclear counterstain.

(D and E) Representative confocal images and quantification of GFAP+ (green) astrocytes in ACC of control and VH rats.

(F and G) Illustrative confocal images and quantification IL1β + (green) of inflammatory cytokines in ACC of control and VH rats.

(H and I) Representative IHC and analysis of S100β+ astrocytes in ACC of control and VH rat.

(J) Western blot for interleukin 1 beta (IL1-β and β-actin) in the ACC of control and VH rats. Mean IL1-β intensity normalized with control revealed that higher expression of IL1-β in VH rats compared to control.

(K) Western blotting (WB) of GFAP and α-tubulin in the ACC. Mean GFAP intensity normalized with control revealed that higher expression of GFAP in VH rats compared to control.

Scale bars: (A left) 250 μm, (A right) 50 μm (B, D, F, and H) 50 μm

Data are presented as mean ± SEM (**p < 0.01, ***p < 0.001 by Unpaired two-tailed Student's *t* test).

Clemastine treatment rescues impaired decision-making in VH and enhances the generation of mature myelin forming OLs

We devised two strategies to determine whether ACC myelin plasticity is necessary for decision-making in rats. First, to identify the physiological role of myelination in ACC, we performed a study of *de novo* focal demyelination (DM) by injecting 1% *LPC*[31] into the rat's ACC region. The level of LPC-induced focal demyelination is greater than that of VH induced hypomyelination (Figures S1A and S1B). The proportion of

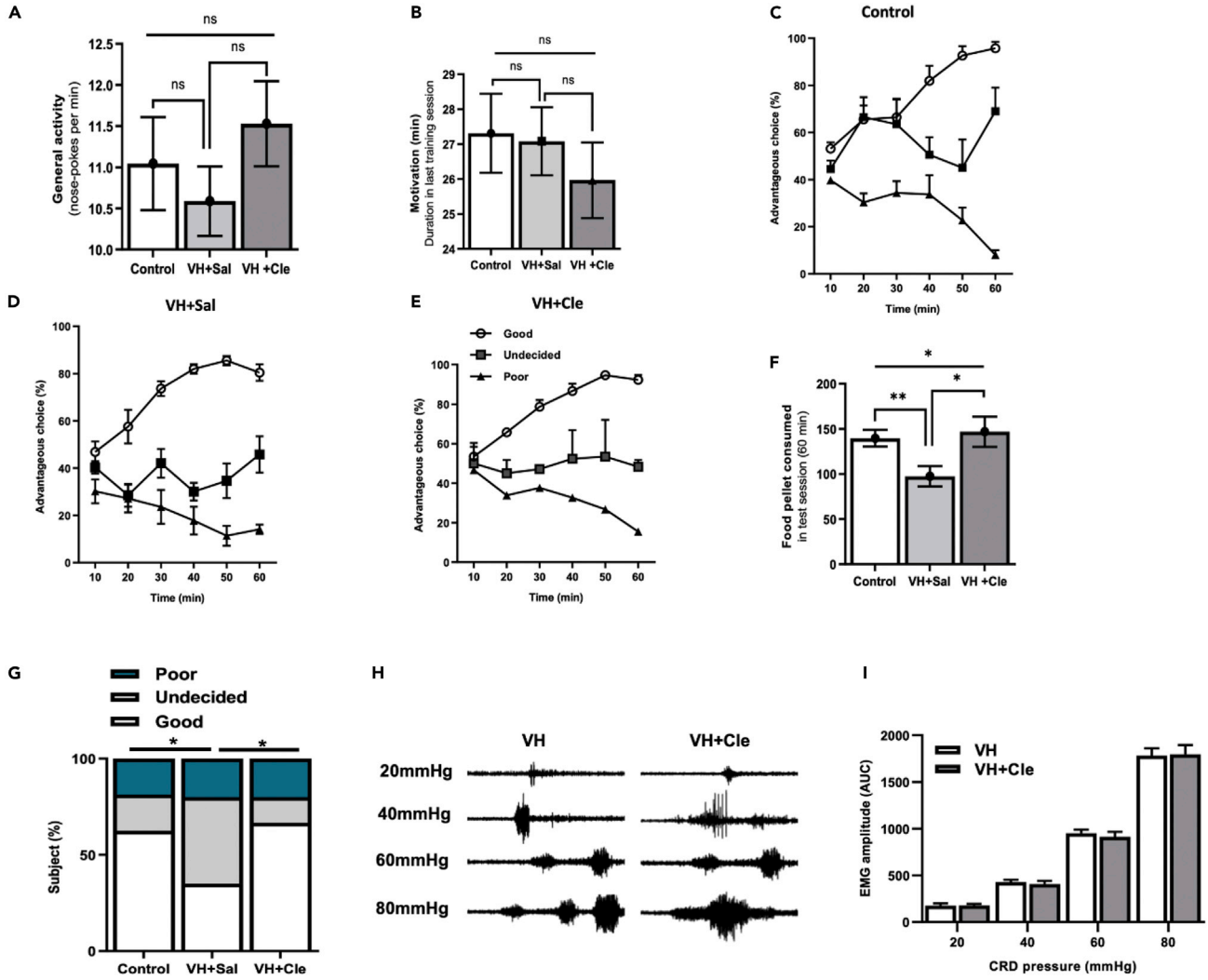

Figure 4. Impairment of decision-making in visceral hypersensitivity rats can be rescued by clemastine treatment

(A and B) The general activities and motivation shows no significant differences among all three group.

(C–E) Identification of good, undecided, and poor decision makers in control (n = 27, C), VH (n = 31, D) and VH + Cle (n = 31, E) during RGT.

(F) The proportions of different types of decision makers in the three groups (*$p < 0.05$, **$p < 0.01$, by Kruskal-Wallis test followed by Dunn-Bonferroni's test for post hoc comparisons).

(G) The food pellets obtained during the test session in all three groups (*$p < 0.05$, by unpaired two-tailed Student's *t* test).

(H) Representative visceromotor response (VMR) recordings to graded pressures of colorectal distension (CRD; 20, 40, 60, 80 mmHg) in saline and clemastine treated VH rats.

(I) The mean amplitudes of electromyography (EMG) in response to graded CRDs were similar in saline and clemastine treated VH rats.

Data are presented as mean ± SEM.

poor decision-makers was increased, and the proportion of good decision-makers and total food consumption was significantly decreased in the DM rats (Figures S1E and S1F), mimicking the impairment found in the chronic pain state, further supporting the idea that myelin plasticity is necessary for cognitive performance in normal and pathophysiological conditions. Second, in separate pharmacologic study, we targeted ACC myelination using clemastine which is the leading drug candidate for myelin formation approved by the Food and Drug Administration (Deshmukh et al., 2013). We found that in clemastine-treated VH rats, the proportion of good decision-makers was increased to 69.5% (Figure 4F). The difference in proportions of the three behavioral subgroups (Figure 4F) and total food consumption (Figure 4G) between two groups was significant. In addition, we found that clemastine treatment had no effect on the visceral pain sensation (Figures 4H and 4I).

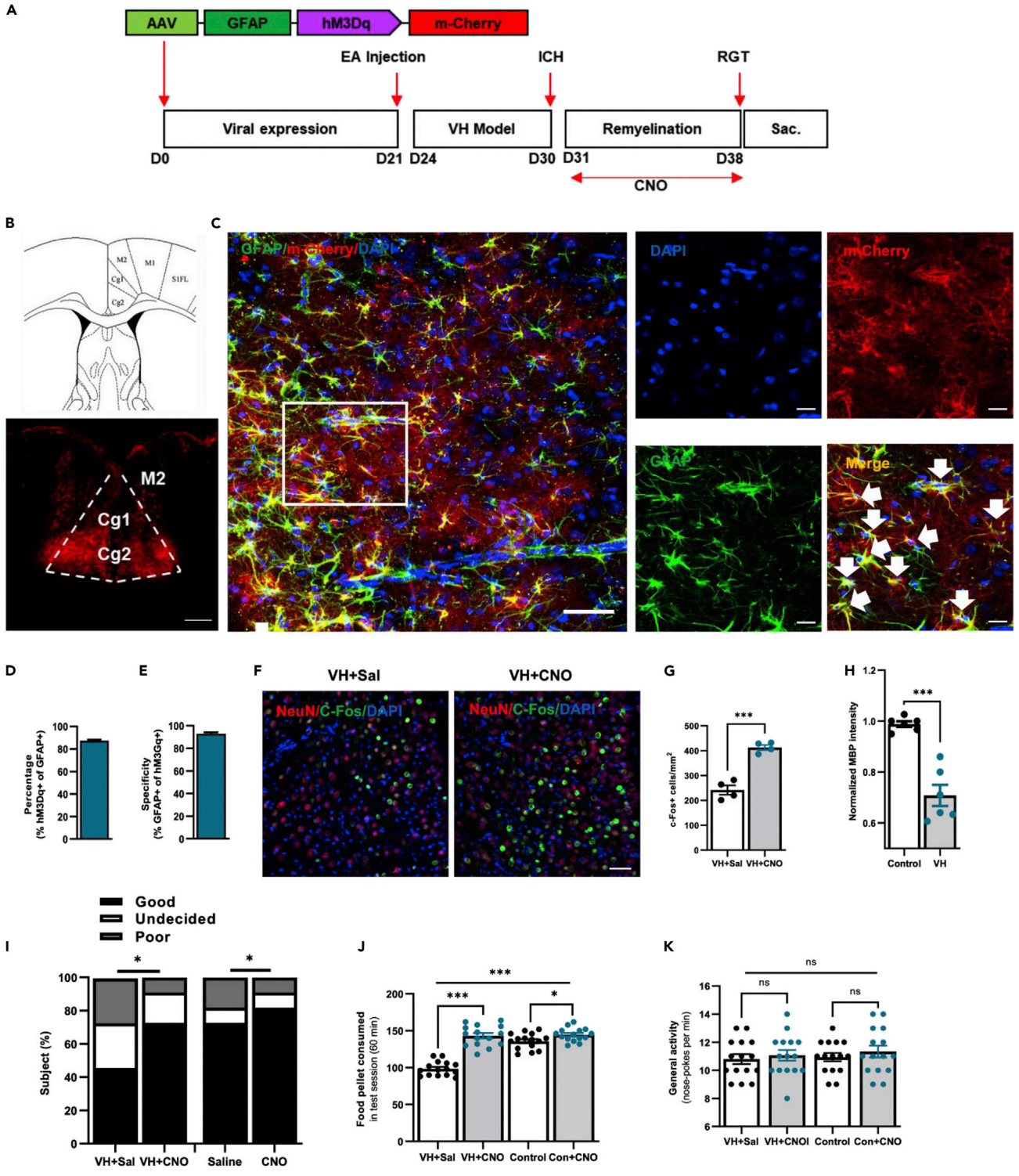

Figure 5. Chemogenetic activation of ACC astrocytes rescues decision making deficits in VH rats

(A) Schematic picture of the timeline of the virus injection and experimental outline of vehicle and CNO injection followed by RGT.

(B) Schematic drawing showing the location of ACC in a coronal brain slice and bilateral injection of AAV8-GFAP:hM3Dq-mCherry virus resulted in the selective expression of hM3Di in the ACC.

(C) hM3Dq (red) was expressed in the astrocytic membrane (green) around the soma and in the distal processes (left). White arrow indicates co-localization of hM3Dq virus with astrocytes in higher magnification (right).

Figure 5. *Continued*

(D and E) GFAP:hM3Dq was expressed in >87% of CA1 astrocytes (512/587 cells from 4 rats; D), with >96% specificity (512/532 cells, from 4 rats; E).

(F and G) CNO administration *in vivo* resulted in a significant increase in c-Fos expression co-labeled with NeuN in the ACC of hM3Dq expressing rats compared to saline treated rats.

(H) Immunostaining with MBP after VH induction shows lower MBP expression in VH rat.

(I) The proportions of different types of decision makers in the four groups (*$p < 0.05$, two-way repeated measures ANOVA).

(J) The food pellets obtained during the testing session in the four groups.

(K) The general activities show no significant difference among the four treated groups.

Scale bars: (B) 500 μm; (C) left 50 μm and right 20 μm; (F) 50 μm

Data are presented as mean ± SEM (**$p < 0.01$, ***$p < 0.001$ by unpaired two-tailed Student's *t* test).

Immunohistochemistry and western blot data revealed a higher intensity of MBP^+ fibers, and significantly increase of the density of myelinated axons in clemastine-treated VH rats (Figures S2A–S2D and S2E–S2H) whereas the thickness of axons remained unchanged in all three groups (Figure S2I). Here, we observed significant increases of the number of $NG2^+$ cells and the newly generating OPCs (Figures S3A–S3D) in the clemastine-treated VH rats relative to saline-treated rats, indicating that clemastine enhances OPC proliferation. Similarly, we identified significant increases in the number of oligodendrocyte cells (Olig2+/CC1+) in clemastine-treated VH compared to saline-treated VH rats (Figures S3E and S3F) and enhanced OPC proliferation, differentiation and the generation of mature myelin forming OLs that could account for the remyelination.

Chemogenetic activation of ACC astrocytes rescues decision-making deficits in VH rats

It has been shown that hM3D(Gq) activation in astrocytes induced NMDA-dependent de novo long-term potentiation in the HPC, and chemogenetic Gq activation of BLA astrocytes promoted fear memory formation via BLA-mPFC communication.[75] In light of our finding that under physiological conditions and pain state, optogenetic activation of astrocytes facilitated synchrony of ACC circuitry (Wang et al., 2017), we utilized the chemogenetic technique to investigate the effect of direct *in vivo* astrocytic activation in cognitive function. Specifically, we delivered an adeno associated virus serotype 8 (AAV8) vector encoding hM3Dq tagged with mCherry under the control of GFAP promoter (AAV8-GFAP:hM3Dq-mCherry) into the ACC (Figures 5A–5C). The expression of hM3Dq has high transfection efficiency (87%) (Figure 5D) and higher specificity (>92%) (Figure 5E). Co-staining with the neuronal nuclei (NeuN) and microglial marker CD68 showed <4% overlap with hM3Dq expression (Figure S4). To verify astrocytic activation *in vivo*, we injected CNO (3 mg/kg, i.p.) 4 weeks after surgery and stained for the immediate-early gene cFos. CNO dramatically increased cFos levels in CNO-treated rats, compared to saline-treated controls (Figures 5F and 5G). To test how astrocytic activation affect decision-making abilities, we injected AAV8-GFAP:hM3Dq-mCherry bilaterally into the ACC. Three weeks later, VH induction was performed (Figure 5A). CNO was administered 30 min before each day of RGT training and testing. The proportion of three subgroups of decision makers among the four treated populations was significantly different (Figure 5H). *Post hoc* analysis revealed that the proportions of the three subgroups of decision makers were significantly different in both CNO-treated control, and VH rats compared with saline group. The final reward gain was also significantly different in the four groups (Figure 5I). However, the general activities in these four groups were similar (Figure 5J). These results suggest that manipulation of AAC astrocytes rescues the decision-making deficit of VH rats.

Astrocytic Gq pathway activation in the ACC induces OPC proliferation, differentiation and enhances oligodendrogenesis, OLs maturation and myelination

To determine whether astrocytic chemogenetic activation induces OPC proliferation and differentiation, we co-administered CNO and EdU in VH and control rats for 10–14 consecutive days before perfusion fixation (Figure 6A). VH rats treated with CNO displayed an overall increase in the density of NG2+ OPC cells (Figures 6B and 6C) as well as increase in the density of mitotically active EdU+/NG2+ OPCs (Figures 6B–6D) relative to saline controls. In addition, an overall increase of oligodendrocyte cell labeled with mature oligodendrocyte marker CC1 was observed in the ACC of CNO-treated VH and control group compared to saline-treated VH and control (Figures 6E and 6F). This increase in oligodendrocyte density was likely because of enhanced OPC differentiation, as CNO-treated VH rats showed a 70.61% increase in the density of EdU+/CC1+ cells (Figure 6F) compared to saline controls. We conduct a similar experiment using viral approach to the normal animals and observed similar effects on OPC proliferation, differentiation and oligodendrogenesis after 10 days of stimulation (Figure S5). To see whether astrocytic Gq activation can enhance remyelination in VH rat, we stained MBP marker 10–14 days after CNO

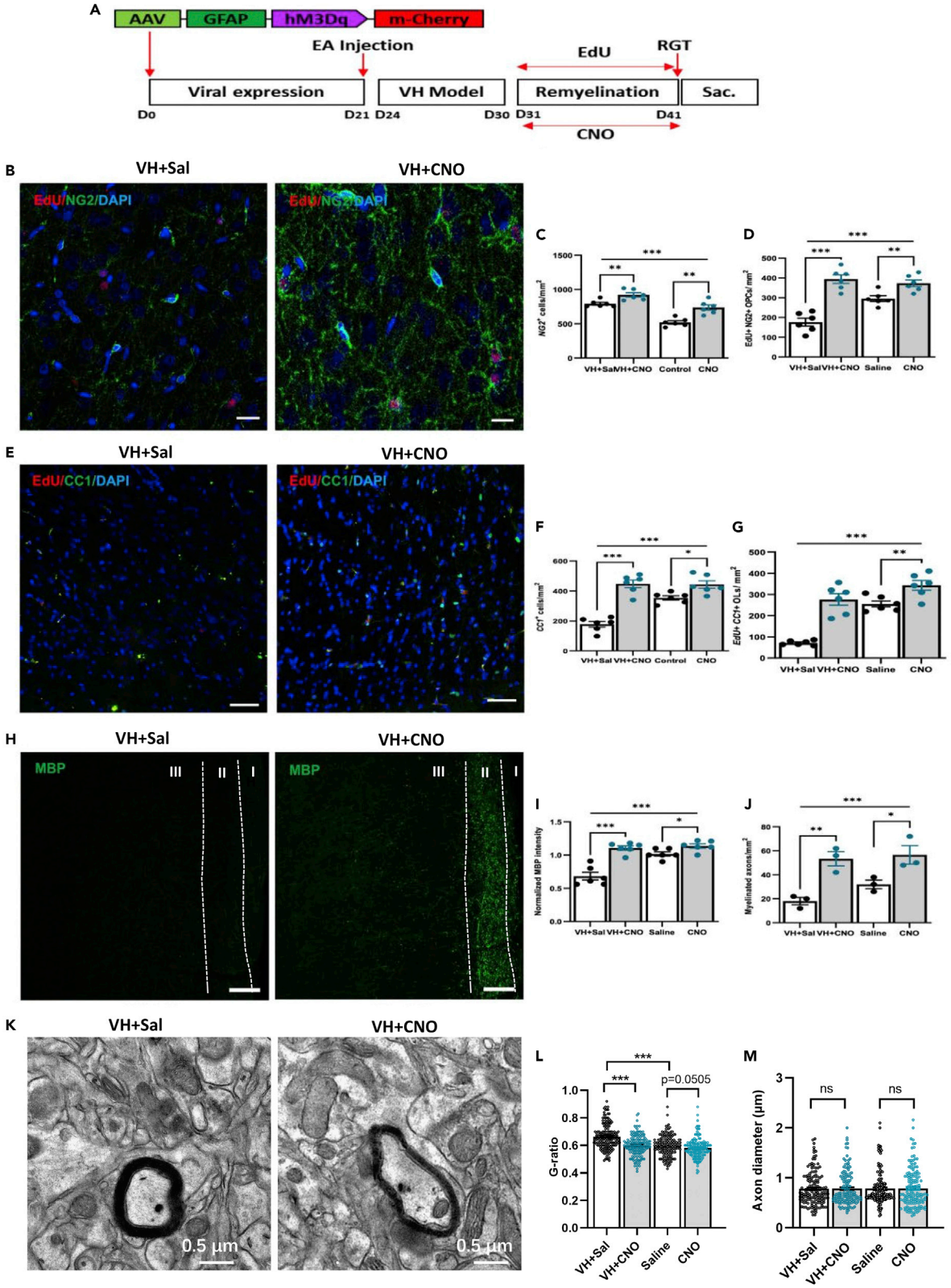
A
AAV
GFAP
hM3Dq
m-Cherry
EA Injection
EdU
RGT
Viral expression
VH Model
Remyelination
Sac.
D0
D21
D24
D30
D31
D41
CNO
B
VH+Sal
VH+CNO
EdU/NG2/DAPI
C
D
E
EdU/CC1/DAPI
F
G
H
MBP
III
II
I
I
J
K
0.5 μm
L
M
p=0.0505
ns
G-ratio
Axon diameter (μm)
Normalized MBP intensity
Myelinated axons/mm²
VH+Sal
VH+CNO
Saline
CNO
Control

Figure 6. Astrocytic Gq pathway activation in the ACC induces OPC proliferation, differentiation and enhances oligodendrogenesis, OLs maturation and myelination

(A) Experimental timeline illustrating onset of CNO/EDU administration in VH rats.

(B–D) Triple IHC and quantification of NG2+ (green) and EdU+ (red) OPCs with an overlay of DAPI (blue) in ACC of saline and CNO treated hM3Dq expressing rats. Graph represents quantification of NG2+ (C) and EdU+ (D) cells per surface area.

(E–G) Triple IHC and quantification of CC1+ (green) and EdU+ (red) OLs with an overlay of DAPI (blue) in ACC of saline and CNO treated hM3Dq expressing rats. Graph represents quantification of CC1+ (F) and EdU+ (G) cells per surface area.

(H–J) Representative confocal images and quantification of MBP+ fibers (green) in ACC of saline and CNO treated hM3Dq expressing rats.

(K) Electron micrographs (EM) of ACC region showing myelinated axons in saline and CNO treated VH rats (n = 5 rats per group).

(L and M) Average G-ratio of myelinated axons in the ACC region of saline and CNO treated VH and control, saline treated hM3Dq expressing rats. No significant changes in the axon diameter among all groups (unpair Student's *t* test, $p > 0.05$).

Scale bars: (B) 20 μm; (E and H) 50 μm; (K) 500 nm

Data are presented as mean ± SEM (*$p < 0.05$, **$p < 0.01$, ***$p < 0.001$ by unpaired two-tailed Student's *t* test).

stimulation and observed higher MBP expression in the ACC of CNO-treated VH and normal rats (Figures 6H and 6I) compared to saline-treated VH and control rats (Figure S5). Ultrastructural analysis further revealed that the density of myelinated axons was significantly increased in CNO treated VH and normal rats in contrast to saline treated VH and control rats (Figures 6J and S5). Quantitative assessment of the G-ratio of myelinated fibers revealed greater thickness of myelin sheath in CNO-treated rats (0.600 ± 0.06) than that in saline-treated rats (0.663 ± 0.07) (Figures 6K and 6L) whereas the thickness of axons remained unchanged in all three groups (Figures 6M and S5). Altogether, our data suggest that astrocytic Gq activation promotes OPC proliferation, differentiation, and generation of new oligodendrocytes in the ACC of VH and normal rat and that this oligodendrogenesis could account for the remyelination.

Chemogenetic activation of astrocytic Gq pathway repairs VH–induced impairments of ACC-amygdala spike-field synchrony

Given that disruptions of ACC-BLA phase-locking and BLA-to-ACC information flow coincide with the poor decision-making performance observed in VH rats,[18,19] we tested whether clemastine treatment in VH rats increased the SFC between ACC spikes and BLA LFP (Figures S6A and S6B). In the VH rats, the averaged SFC values in theta range (4–10 Hz) were significantly decreased from 5.40% ± 0.43%–2.90% ± 0.22% (Figure S6C). Seven days clemastine treatment in VH rats increased the theta SFC to 3.86% ± 0.20%, compared to the saline group, whereas 14 days' clemastine treatment increased the theta SFC values to 5.09 ± 0.23% compared to VH rats. There is no significant difference for clemastine treatment with 14 days compared to controls (Figure S6C). Furthermore, clemastine treatment in VH rats restored the proportion of phase-locking neurons to 19.38% ± 4.29% comparable with the VH-Saline group (Figure S6E). We then analyzed the cross-correlogram between the LFPs recorded in the ACC region and BLA region in all groups of rats (Figure S6F). From the cross-correlograms, we analyzed the second positive peak corresponding to the theta activity. The magnitude of the second positive peak is decreased after VH induction to 0.161 ± 0.0289 from 0.633 ± 0.082 in control rats (Figure S6G). Clemastine treatment for 7 days showed significant increase in the magnitude of correlation value, whereas 14 days clemastine treatment in VH rats also increased the magnitude of second peak to 0.643 ± 0.104 (Figure S6G) indicating the facilitation of synchronization between ACC and BLA. Then, we sought to test whether chemogenetic activation of astrocytic Gq pathway can also rescue the impairment of SFC and phase lock between ACC and BLA. Using another group of rats, we injected chemogenetic virus in ACC and conducted the VH modeling 3 weeks later. Then, we injected CNO or saline for 12 days, and recorded ACC and BLA in anesthetized state (Figures 7A and 7B). We found that VH rats received saline showed impaired SFC between ACC and BLA compared with Ctrl group, whereas VH rats received CNO showed significant increase SFC compared with VH-Sal group (Figure 7C, $p < 0.05$, $p < 0.05$). Also, we confirmed that VH modeling decrease phase lock neurons percentage compared to control group (Figure 7D, $p < 0.01$). In addition, chemogenic activation of astrocytic Gq pathway rescued the decrease of phase lock (Figure 7D $p < 0.05$). Taken together, our data suggest that astrocytic Gq activity in ACC play an important role in ACC-BLA spike-field synchrony.

DISCUSSION

Cognition encapsulates an array of mental processes such as learning, memory, attention, evaluation, decision-making, etc. Psychiatric symptoms attributed to higher order cognitive dysfunctions have been reproduced in behavioral tasks utilizing animal models.[38] The mechanism for myelin plasticity in cognitive performance is yet to be clearly elucidated. Using a multiple flavor-place paired associates (PAs) learning

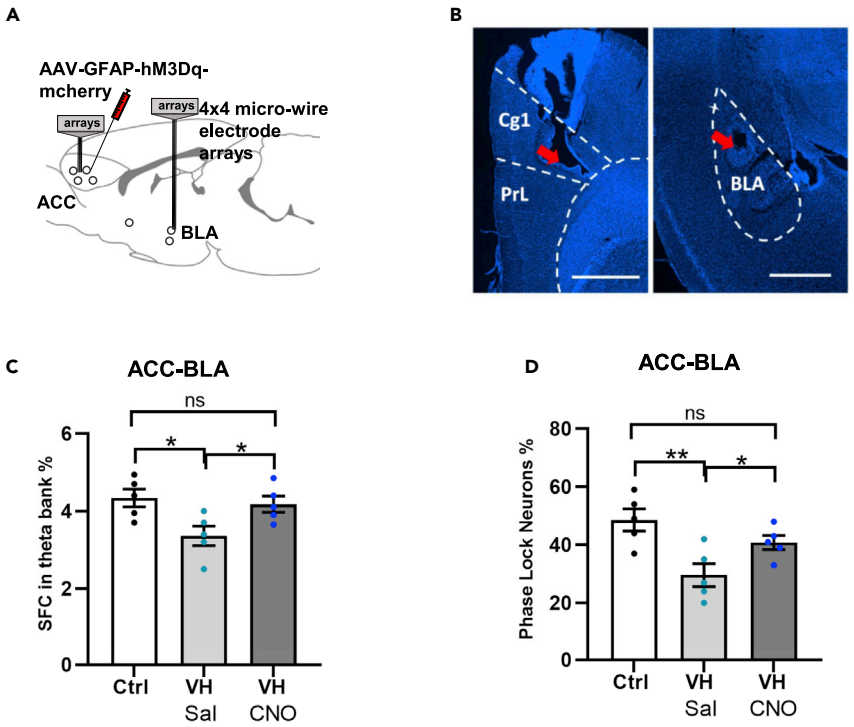

Figure 7. Chemogenetic Gq activation in ACC astrocytes repairs VH–induced impairments of ACC-amygdala spike-field synchrony

(A) Schematic picture of virus injection and electrophysiology recording.

(B) A representative section with DAPI shows microelectrode sites. The red arrows show the placements of ACC and BLA electrode.

(C) Averaged SFC values in theta band in CNO/saline treated VH rats with hm3Dq virus injection and control rats (n = 5 rats each group).

(D) Averaged percentages of phase locked neurons percentage of ACC single-unit spikes phase-locking to BLA theta band field potential in saline/CNO treated VH rats with hm3Dq virus injection and control rats (n = 5 rats each group). Data are presented as mean ± SEM (*p < 0.05, **p < 0.01, by unpaired two-tailed Student's *t* test).

and memory behavioral paradigm, our recent study showed that the establishment of a memory schema is associated with oligodendrogenesis and adaptive myelination within the ACC network. Furthermore, lysolecithin-induced demyelination impaired PAs learning and memory.[31] These findings provide further evidence that myelin plasticity is related to prolonged cognitive performance.

We and other investigators used an animal model of decision-making, the Rat Gambling Task (RGT),[18,19,39–41] and obtained results similar to the findings from the Iowa gambling task (IGT). Consistent with our previous observations, in this study, we showed that the chronic visceral hypersensitivity condition resulted in a higher proportion of poor decision makers and lower proportion of good decision makers among VH rats. We report several novel discoveries to strongly suggest that dysregulation of myelin plasticity occurs in chronic pain. Hypomyelination in the ACC neuronal circuitry may have a significant impact on neural network functioning. Demyelination is the important mechanism underlying impaired decision making in chronic visceral hypersensitivity state.

Neuroinflammation associated with hypomyelination of brain areas in chronic visceral hypersensitivity

A multitude of evidence has shown that CNS myelin alterations are involved in learning and memory processes and have wide-ranging implications for plasticity in the adult neural circuitry. White matter comprises millions of nerve fiber bundles that connect and arrange neurons in different brain regions into functional circuits. The myelin that constitutes white matter provides the electrical insulation to axons; myelin formation continues into adulthood.[1] Several human imaging studies have identified white matter

irregularities in psychiatric conditions including autism, chronic depression, attention-deficit hyperactivity disorder, and Alzheimer's disease.[34,42,43] Adverse experiences such as social isolation,[44] early life stress,[45] maternal high fat diet,[46] or chemotherapy[47] can cause myelination defects, leading to behavioral abnormalities. It is worth noting that studies have established regional gray matter and white matter abnormalities in the brains of patients with irritable bowel syndrome.[6–8]

Increased levels of pro-inflammatory cytokines, such as IL-1β, IL-6 and TNF-α, have been found in patients suffering from depression or chronic pain,[20] and in experimental animal models of neuropathic pain.[21,48] Circulating cytokines may enter the CNS through diffusion through the permeable BBB; they can also be released within the brain by activated glia cells.[48] We showed higher expression of inflammatory cytokines like IL-1β and IL6 in the ACC of rats with trigeminal neuropathy[22] and the VH rats compared to that of control rats (Figures 3C–3E). Increases in the number of reactive microglia were also observed in the ACC of VH rats compared to control (Figures 3A and 3B), which is the possible cause of neuroinflammation. These reactive microglia then rapidly proliferate and respond to infectious and inflammatory stimuli and become phagocytotic for the clearance of pathogens or infections to maintain normal homeostasis. Reactive microglia release substances such as inflammatory cytokines (IL-1β, TNF-α, IL-6), NO, PGE2, ROS and superoxide that cause neuronal damage and contribute to neurodegeneration. Oligodendroglia in rodents and humans are acutely sensitive to inflammation and oxidative stress-induced excitotoxicity.[25,26] Microglia are vital to myelin plasticity because of the phagocytosis of myelin debris, and the secretion of cytokines, chemokines, and soluble mediators at the lesion site. A number of recent studies support the existence of a wide spectrum of microglia activation states.[49] It has been reported that inflammatory mediators and reactive microglial cells activate Notch and Wnt signaling that may hinder OPC differentiation,[50,51] causing hypomyelination. Here, our immunohistochemistry and western blot data demonstrate the reduced expression of myelin basic protein (MBP) in the ACC of VH rats. NG2 cells are one of the most rapidly expanding glial cell populations in the CNS. In the adult brain, oligodendrocyte progenitor cells (OPCs) remain in an inactive form. However, they can be stimulated to undergo proliferation, differentiation and generate mature myelinating oligodendrocytes in response specific circumstances, such as a demyelinating injury, inflammatory condition,[52,53] or chronic hypoxia.[54] In this study, we observed that total number of OPCs ($NG2^+$) cells was increased in VH rats. Conversely, there were a decreased number of matured oligodendrocytes (OLs, CCI^+) in the ACC of VH rats suggesting that the shortage of mature OLs could account for the hypomyelination in VH rats. We also showed decreased cells co-labeling of EdU^+ and $CC1^+$, suggesting impairment of OPCs differentiation and a substantial decrease in the generation of mature OLs in the ACC. Moreover, ultrastructural analysis using electron microscopy revealed that the myelin sheath thickness had been compromised in VH rats, indicating that inhibition of OPC differentiation and impairment of mature myelinating OLs formation result in hypomyelination. Myelin regulatory factor (MyRF) is a transcriptional protein critical for OPCs differentiation into pre-myelinating and myelinating oligodendrocytes, and for the eventual production of mature myelinating OLs.[55,56] We demonstrate that MyRF protein is downregulated in VH rats compare to control. In VH rats, very few oligodendrocytes express MyRF protein ($CC1^+$ $MyRF^+$ OLs). However, whether oligodendrocyte modification is an important component of impaired decision-making is not clear.

Myelin plasticity in oscillations and brain network synchrony

System level brain activity is rhythmic and oscillatory. Neuronal oscillations can synchronize neurons, create coherent cell assemblies,[27,28,57,58] and promote plasticity when pre- and post-synaptic activity are precisely timed.[30]

One of the well-known functions of myelin is to modulate nerve conduction velocity, which in turn regulates nerve and neural network plasticity.[59] Recent computational analysis suggests that conduction delays between coupled oscillators in the brain can be sensitive to minor variations in conduction speed caused by slight changes in myelin.[60] Myelination facilitates long-range oscillations and synchrony of spike time arrival between neurons in different brain areas.[3,29] On the other hand, delicate changes in myelin may cause conduction delays between coupled oscillators in the brain.[29]

Our previously published data indicates that phase locking and synchronization within the ACC and between the ACC and BLA are key to modulating decision-making behavior in rats.[18,19,22,61] How do discrete alterations in myelin morphology impact neural signal conduction in chronic visceral hypersensitivity? It is not known whether oligodendrocyte changes are an important component of impaired decision making.

Pharmacologic targeting of myelin in cognitive performance and brain network synchrony

To clarify the physiological role of myelination in circuit-specific contexts, we perform a study *de novo* demyelination of brain areas. Lysolecithin (LPC) is a detergent-like membrane solubilizing agent.[62] Using normal rats (*in vivo*), we show that demyelination of ACC impairs decision-making, mimicking the impairment found in the chronic pain state, further supporting the idea that myelin plasticity is necessary for cognitive performance in normal and pathophysiological conditions. However, it is unclear whether myelin plasticity propels learning or if changes in myelin are a consequence of the modified neuronal circuits. We provide clear evidence that ACC lysolecithin-induced demyelination lead to a decrease in ACC theta band power and reduced spike-field coherence and phase-locking between ACC spikes and theta phase,[31] suggesting the key role of myelination for long-range oscillations and synchrony of spike time arrival between distant populations of neurons.

In a separate study, clemastine was used to enhance oligodendrocyte myelination. Clemastine is the leading drug candidate for myelin formation approved by Food and Drug Administration.[63] It has been shown to promote OPC differentiation *in vitro*, stimulate remyelination after demyelinating lesions in mice,[64] and prevent the onset of social isolation-induced avoidance behavior by enhancing myelin formation.[65] Here, we observed that daily oral administration of clemastine prevented hypomyelination and potentiated remyelination in the visceral hypersensitivity condition which was associated with improvement in decision-making behavior. Clemastine or chemogenetic activation of astrocytic Gq pathway can restore spike-field coherence and phase-locking between ACC and BLA in the VH rats. Our findings support an elegant study that evidenced bidirectional manipulation of myelin plasticity affects neural activity during fear learning suggesting that delicate modifications to myelin structure can facilitate optimal function within the neuronal circuit.[66]

Astroglia activity promotes oligodendrogenesis and adaptive myelination

Oligodendrocytes are responsible for remyelination, a process regulated by intrinsic pathways and facilitated by extrinsic factors from surrounding cells.[29] Astrocyte populations can be connected in unison to allow collective metabolic and electric coupling, as well as calcium-wave signaling.[67] Astrocytes are capable of releasing major neurotransmitters: glutamate, ATP, GABA, and glycine.[68,69]

It has been well documented that excitatory neuronal activity initiates myelination, OPC proliferation, and differentiation.[32] On the other hand, blocking neuronal activity has been shown to decrease OPC proliferation.[70] Astrocytes support neuronal functions by providing neuronal energy substrates such as lactate by means of their astrocytic processes.[19,71] Oligodendrocytes, which can consume lactate via monocarboxylate transporters, take up lactate at a greater rate than other CNS cells.[72] In addition to supporting neuronal survival and maintenance evidences have shown that astrocytes promote myelin structure and conduction velocity[29] through astrocytes Ca^{2+}-evoked ATP release[73] and their direct involvement in the proliferation, differentiation and migration of oligodendrocytes.[36] In this study, we showed that astrocytic Gq activation promotes OPC proliferation, differentiation, and generation of new oligodendrocytes in the ACC of VH and normal rats. Ultrastructural analysis further clarified the significant increases in the density of myelinated axons in CNO-treated VH and normal rats. These findings support recent reports concerning the ability of glial cells to promote OPCs to stimulate remyelination after the loss or damage of myelin.[37] The role of perinodal astrocytes in regulating myelin structure and conduction velocity has been recently identified.[29] Note that with the present study, we may not be able to distinguish between different possibilities of whether astrocytes Gq activation or clemastine treatment led to enhance myelination of hypomyelinated axons in VH state or whether new myelin formed by existing or new OLs increase the thickness of the myelin sheath. Further studies are needed to expand our understanding on the mechanism underlying myelination and remyelination.

In conclusion, hypomyelination in ACC is an important component of impaired decision-making behavior in visceral hypersensitivity. Astroglia activation promotes oligodendrogenesis and adaptive myelination. Enhancing oligodendrocyte myelination by chemogenetic activation of astrocytes restores long-range theta-frequency oscillations and synchrony of spike time arrival between neurons in BLA-ACC. Our results suggest that myelination-enhancing strategies present a novel therapeutic approach for the rescue of cognitive deficits in the chronic pain state.

Limitations of the study

As already noted in the discussion, we may not be able to distinguish between different possibilities of whether Gq activation in astrocytes led to enhance myelination of hypomyelinated axons in VH state or whether new

myelin formed by existing or new OLs increase the thickness of the myelin sheath. Further studies are needed to expand our understanding on the mechanism underlying myelination and remyelination.

STAR★METHODS

Detailed methods are provided in the online version of this paper and include the following:

- KEY RESOURCES TABLE
- RESOURCE AVAILABILITY
  - Lead contact
  - Materials availability
  - Data and code availability
- EXPERIMENTAL MODEL AND SUBJECT DETAILS
  - Animals and ethical consideration
  - Visceral hypersensitivity (VH) rat model
  - Focal demyelination
  - Drug (clemastine) induced remyelination
  - Chemogenetic activation of astrocytic Gq pathway
  - *In vivo* electrophysiology recordings
- METHOD DETAILS
  - Development of VH animal model
  - Surgery
  - Viral injection
  - Focal demyelination
  - Drug Administration
  - Rat gambling task (RGT)
  - Immunohistochemistry
  - Confocal imaging and processing
  - Protein extraction and western blot analysis
  - TEM microscopy
  - Multiple-channel electrophysiology recording in ACC and BLA
- QUANTIFICATION AND STATISTICAL ANALYSIS

SUPPLEMENTAL INFORMATION

Supplemental information can be found online at https://doi.org/10.1016/j.isci.2022.105840.

ACKNOWLEDGMENTS

We thank Bing He for TEM technical support. This work was supported by the Research Grants Council of Hong Kong (11103721, 11102820, and 11100018), the National Natural Science Foundation of China (NSFC) and RGC Joint Research Scheme (3171101014, N_CityU114/17), HEALTH@InnoHK Program launched by the Innovation and Technology Commission of the Hong Kong SAR, China (CityU 9445909), the Shenzhen-Hong Kong Institute of Brain Science Innovation Open Project Contract (NYKFKT2019012). This work was also supported by City University of Hong Kong Neuroscience Research Infrastructure Grant (9610211), and Centre for Biosystems, Neuroscience, and Nanotechnology Grant (9360148).

AUTHOR CONTRIBUTIONS

Conceptualization, Y.L.; Methodology, M.H., Z.L., and Y.L.; Validation, M.H. and Z.L.; Investigation, M.H., Z.L., M.A., Z.I., and F.U.; Writing – Original Draft, M.H., Z.L., and Y.L.; Writing – Review and Editing, Z.L., A.S.R., and Y.L.; Funding Acquisition, Y.L.; Supervision, Y.L. The authors read and approved the final manuscript.

DECLARATION OF INTERESTS

The authors declare no competing interests.

INCLUSION AND DIVERSITY

We support inclusive, diverse, and equitable conduct of research.

Received: November 30, 2021
Revised: April 20, 2022
Accepted: December 16, 2022
Published: January 20, 2023

REFERENCES

1. Hill, R.A., Li, A.M., and Grutzendler, J. (2018). Lifelong cortical myelin plasticity and age-related degeneration in the live mammalian brain. Nat. Neurosci. *21*, 683–695. https://doi.org/10.1038/s41593-018-0120-6.

2. Fields, R.D. (2010). Change in the brain's white matter. Science *330*, 768–769. https://doi.org/10.1126/science.1199139.

3. Fields, R.D. (2015). A new mechanism of nervous system plasticity: activity-dependent myelination. Nat. Rev. Neurosci. *16*, 756–767. https://doi.org/10.1038/nrn4023.

4. McKenzie, I.A., Ohayon, D., Li, H., De Faria, J.P., Emery, B., Tohyama, K., and Richardson, W.D. (2014). Motor skill learning requires active central myelination. Science *346*, 318–322. https://doi.org/10.1126/science.1254960.

5. Zatorre, R.J., Fields, R.D., and Johansen-Berg, H. (2012). Plasticity in gray and white: neuroimaging changes in brain structure during learning. Nat. Neurosci. *15*, 528–536. https://doi.org/10.1038/nn.3045.

6. Chen, J.Y.-W., Blankstein, U., Diamant, N.E., and Davis, K.D. (2011). White matter abnormalities in irritable bowel syndrome and relation to individual factors. Brain Res. *1392*, 121–131. https://doi.org/10.1016/j.brainres.2011.03.069.

7. Ellingson, B.M., Mayer, E., Harris, R.J., Ashe-McNally, C., Naliboff, B.D., Labus, J.S., and Tillisch, K. (2013). Diffusion tensor imaging detects microstructural reorganization in the brain associated with chronic irritable bowel syndrome. Pain *154*, 1528–1541. https://doi.org/10.1016/j.pain.2013.04.010.

8. Gupta, G., Gelfand, J.M., and Lewis, J.D. (2005). Increased risk for demyelinating diseases in patients with inflammatory bowel disease. Gastroenterology *129*, 819–826. https://doi.org/10.1053/j.gastro.2005.06.022.

9. Gao, J., Wu, X., Owyang, C., and Li, Y. (2006). Enhanced responses of the anterior cingulate cortex neurones to colonic distension in viscerally hypersensitive rats. J. Physiol. *570*, 169–183. https://doi.org/10.1113/jphysiol.2005.096073.

10. Ness, T.J., and Gebhart, G.F. (1990). Visceral pain: a review of experimental studies. Pain *41*, 167–234. https://doi.org/10.1016/0304-3959(90)90021-5.

11. Nozdrachev, A.D., Akoev, G.N., Filippova, L.V., Sherman, N.O., Lioudyno, M.I., and Makarov, F.N. (1999). Changes in afferent impulse activity of small intestine mesenteric nerves in response to antigen challenge. Neuroscience *94*, 1339–1342. https://doi.org/10.1016/S0306-4522(99)00377-2.

12. Cao, Z., Wu, X., Chen, S., Fan, J., Zhang, R., Owyang, C., and Li, Y. (2008). Anterior cingulate cortex modulates visceral pain as measured by visceromotor responses in viscerally hypersensitive rats. Gastroenterology *134*, 535–543. https://doi.org/10.1053/j.gastro.2007.11.057.

13. Fan, J., Wu, X., Cao, Z., Chen, S., Owyang, C., and Li, Y. (2009). Up-regulation of anterior cingulate cortex NR2B receptors contributes to visceral pain responses in rats. Gastroenterology *136*, 1732–1740.e3. https://doi.org/10.1053/j.gastro.2009.01.069.

14. Wang, J., Zhang, X., Cao, B., Liu, J., and Li, Y. (2015). Facilitation of synaptic transmission in the anterior cingulate cortex in viscerally hypersensitive rats. Cereb. Cortex *25*, 859–868. https://doi.org/10.1093/cercor/bht273.

15. Wu, X., Gao, J., Yan, J., Fan, J., Owyang, C., and Li, Y. (2008). Role for NMDA receptors in visceral nociceptive transmission in the anterior cingulate cortex of viscerally hypersensitive rats. Am. J. Physiol. Gastrointest. Liver Physiol. *294*, G918–G927. https://doi.org/10.1152/ajpgi.00452.2007.

16. Icenhour, A., Langhorst, J., Benson, S., Schlamann, M., Hampel, S., Engler, H., Forsting, M., and Elsenbruch, S. (2015). Neural circuitry of abdominal pain-related fear learning and reinstatement in irritable bowel syndrome. Neuro Gastroenterol. Motil. *27*, 114–127. https://doi.org/10.1111/nmo.12489.

17. Apkarian, A.V., Lavarello, S., Randolf, A., Berra, H.H., Chialvo, D.R., Besedovsky, H.O., and del Rey, A. (2006). Expression of IL-1β in supraspinal brain regions in rats with neuropathic pain. Neurosci. Lett. *407*, 176–181. https://doi.org/10.1016/j.neulet.2006.08.034.

18. Cao, B., Wang, J., Mu, L., Poon, D.C.H., and Li, Y. (2016). Impairment of decision making associated with disruption of phase-locking in the anterior cingulate cortex in viscerally hypersensitive rats. Exp. Neurol. *286*, 21–31. https://doi.org/10.1016/j.expneurol.2016.09.010.

19. Wang, J., Tu, J., Cao, B., Mu, L., Yang, X., Cong, M., Ramkrishnan, A.S., Chan, R.H.M., Wang, L., and Li, Y. (2017). Astrocytic L-lactate signaling facilitates amygdala-anterior cingulate cortex synchrony and decision making in rats. Cell Rep. *21*, 2407–2418. https://doi.org/10.1016/j.celrep.2017.11.012.

20. Backonja, M.M., Coe, C.L., Muller, D.A., and Schell, K. (2008). Altered cytokine levels in the blood and cerebrospinal fluid of chronic pain patients. J. Neuroimmunol. *195*, 157–163. https://doi.org/10.1016/j.jneuroim.2008.01.005.

21. Xie, W., Luo, S., Xuan, H., Chou, C., Song, G., Lv, R., Jin, Y., Li, W., and Xu, J. (2006). Betamethasone affects cerebral expressions of NF-κB and cytokines that correlate with pain behavior in a rat model of neuropathy. Ann. Clin. Lab. Sci. *36*, 39–46.

22. Murugappan, S.K., Xie, L., Wong, H.Y., Iqbal, Z., Lei, Z., Ramkrishnan, A.S., and Li, Y. (2021). Suppression of pain in the late phase of chronic trigeminal neuropathic pain failed to rescue the decision-making deficits in rats. Int. J. Mol. Sci. *22*, 7846. https://doi.org/10.3390/ijms22157846.

23. Thion, M.S., Ginhoux, F., and Garel, S. (2018). Microglia and early brain development: an intimate journey. Science *362*, 185–189. https://doi.org/10.1126/science.aat0474.

24. Costa, G.M.F., de Oliveira, A.P., Martinelli, P.M., da Silva Camargos, E.R., Arantes, R.M.E., and de Almeida-Leite, C.M. (2016). Demyelination/remyelination and expression of interleukin-1β, substance P, nerve growth factor, and glial-derived neurotrophic factor during trigeminal neuropathic pain in rats. Neurosci. Lett. *612*, 210–218. https://doi.org/10.1016/j.neulet.2015.12.017.

25. Deng, W. (2010). Neurobiology of injury to the developing brain. Nat. Rev. Neurol. *6*, 328–336. https://doi.org/10.1038/nrneurol.2010.53.

26. Juurlink, B.H. (1997). Response of glial cells to Ischemia: roles of reactive oxygen species and glutathione. Neurosci. Biobehav. Rev. *21*, 151–166. https://doi.org/10.1016/S0149-7634(96)00005-X.

27. Buzsáki, G., and Draguhn, A. (2004). Neuronal oscillations in cortical networks. Science *304*, 1926–1929. https://doi.org/10.1126/science.1099745.

28. Padilla-Coreano, N., Canetta, S., Mikofsky, R.M., Alway, E., Passecker, J., Myroshnychenko, M.V., Garcia-Garcia, A.L., Warren, R., Teboul, E., Blackman, D.R., et al. (2019). Hippocampal-Prefrontal theta transmission regulates avoidance behavior. Neuron *104*, 601–610.e4. https://doi.org/10.1016/j.neuron.2019.08.006.

29. Dutta, D.J., Woo, D.H., Lee, P.R., Pajevic, S., Bukalo, O., Huffman, W.C., Wake, H., Basser, P.J., SheikhBahaei, S., Lazarevic, V., et al. (2018). Regulation of myelin structure and conduction velocity by perinodal astrocytes. Proc. Natl. Acad. Sci. USA *115*, 11832–11837. https://doi.org/10.1073/pnas.1811013115.

30. Markram, H., Lübke, J., Frotscher, M., and Sakmann, B. (1997). Regulation of synaptic efficacy by coincidence of postsynaptic APs and EPSPs. Science *275*, 213–215. https://doi.org/10.1126/science.275.5297.213.

31. Hasan, M., Kanna, M.S., Jun, W., Ramkrishnan, A.S., Iqbal, Z., Lee, Y., and Li, Y. (2019). Schema-like learning and memory consolidation acting through myelination. FASEB J. *33*, 11758–11775. https://doi.org/10.1096/fj.201900910R.

32. Gibson, E.M., Purger, D., Mount, C.W., Goldstein, A.K., Lin, G.L., Wood, L.S., Inema, I., Miller, S.E., Bieri, G., Zuchero, J.B., et al. (2014). Neuronal activity promotes oligodendrogenesis and adaptive myelination in the mammalian brain. Science *344*, 1252304. https://doi.org/10.1126/science.1252304.

33. Duman, R.S., Aghajanian, G.K., Sanacora, G., and Krystal, J.H. (2016). Synaptic plasticity and depression: new insights from stress and rapid-acting antidepressants. Nat. Med. *22*, 238–249. https://doi.org/10.1038/nm.4050.

34. Fields, R.D. (2008). White matter in learning, cognition and psychiatric disorders. Trends Neurosci. *31*, 361–370. https://doi.org/10.1016/j.tins.2008.04.001.

35. Nagai, J., Yu, X., Papouin, T., Cheong, E., Freeman, M.R., Monk, K.R., Hastings, M.H., Haydon, P.G., Rowitch, D., Shaham, S., and Khakh, B.S. (2021). Behaviorally consequential astrocytic regulation of neural circuits. Neuron *109*, 576–596. https://doi.org/10.1016/j.neuron.2020.12.008.

36. Tognatta, R., Karl, M.T., Fyffe-Maricich, S.L., Popratiloff, A., Garrison, E.D., Schenck, J.K., Abu-Rub, M., and Miller, R.H. (2020). Astrocytes are required for oligodendrocyte survival and maintenance of myelin compaction and integrity. Front. Cell. Neurosci. *14*, 74–147. https://doi.org/10.3389/fncel.2020.00074.

37. Traiffort, E., Kassoussi, A., Zahaf, A., and Laouarem, Y. (2020). Astrocytes and microglia as major players of myelin production in normal and pathological conditions. Front. Cell. Neurosci. *14*, 79. https://doi.org/10.3389/fncel.2020.00079.

38. Nestler, E.J., and Hyman, S.E. (2010). Animal models of neuropsychiatric disorders. Nat. Neurosci. *13*, 1161–1169. https://doi.org/10.1038/nn.2647.

39. Fugariu, V., Zack, M.H., Nobrega, J.N., Fletcher, P.J., and Zeeb, F.D. (2020). Effects of exposure to chronic uncertainty and a sensitizing regimen of amphetamine injections on locomotion, decision-making, and dopamine receptors in rats. Neuropsychopharmacology *45*, 811–822. https://doi.org/10.1038/s41386-020-0599-x.

40. Georgiou, P., Zanos, P., Bhat, S., Tracy, J.K., Merchenthaler, I.J., McCarthy, M.M., and Gould, T.D. (2018). Dopamine and stress system modulation of sex differences in decision making. Neuropsychopharmacology *43*, 313–324. https://doi.org/10.1038/npp.2017.161.

41. Zeeb, F.D., and Winstanley, C.A. (2011). Lesions of the basolateral amygdala and orbitofrontal cortex differentially affect acquisition and performance of a rodent gambling task. J. Neurosci. *31*, 2197–2204. https://doi.org/10.1523/JNEUROSCI.5597-10.2011.

42. Bolkan, S., and Gordon, J.A. (2016). Untangling autism. Nature *532*, 45–46. https://doi.org/10.1038/nature17311.

43. Nave, K.-A., and Ehrenreich, H. (2014). Myelination and oligodendrocyte functions in psychiatric diseases. JAMA Psychiatr. *71*, 582–584. https://doi.org/10.1001/jamapsychiatry.2014.189.

44. Liu, J., Dietz, K., Deloyht, J.M., Pedre, X., Kelkar, D., Kaur, J., Vialou, V., Lobo, M.K., Dietz, D.M., Nestler, E.J., et al. (2012). Impaired adult myelination in the prefrontal cortex of socially isolated mice. Nat. Neurosci. *15*, 1621–1623. https://doi.org/10.1038/nn.3263.

45. Yang, Y., Cheng, Z., Tang, H., Jiao, H., Sun, X., Cui, Q., Luo, F., Pan, H., Ma, C., and Li, B. (2017). Neonatal maternal separation impairs prefrontal cortical myelination and cognitive functions in rats through activation of Wnt signaling. Cereb. Cortex *27*, 2871–2884. https://doi.org/10.1093/cercor/bhw121.

46. Graf, A.E., Lallier, S.W., Waidyaratne, G., Thompson, M.D., Tipple, T.E., Hester, M.E., Trask, A.J., and Rogers, L.K. (2016). Maternal high fat diet exposure is associated with increased hepcidin levels, decreased myelination, and neurobehavioral changes in male offspring. Brain Behav. Immun. *58*, 369–378. https://doi.org/10.1016/j.bbi.2016.08.005.

47. Geraghty, A.C., Gibson, E.M., Ghanem, R.A., Greene, J.J., Ocampo, A., Goldstein, A.K., Ni, L., Yang, T., Marton, R.M., Paşca, S.P., et al. (2019). Loss of adaptive myelination contributes to methotrexate chemotherapy-related cognitive impairment. Neuron *103*, 250–265.e8. https://doi.org/10.1016/j.neuron.2019.04.032.

48. Vezzani, A., and Viviani, B. (2015). Neuromodulatory properties of inflammatory cytokines and their impact on neuronal excitability. Neuropharmacology *96*, 70–82. https://doi.org/10.1016/j.neuropharm.2014.10.027.

49. Fernández-Arjona, M.D.M., Grondona, J.M., Fernández-Llebrez, P., and López-Ávalos, M.D. (2019). Microglial morphometric parameters correlate with the expression level of IL-1β, and allow identifying different activated morphotypes. Front. Cell. Neurosci. *13*, 472. https://doi.org/10.3389/fncel.2019.00472.

50. Fancy, S.P.J., Harrington, E.P., Yuen, T.J., Silbereis, J.C., Zhao, C., Baranzini, S.E., Bruce, C.C., Otero, J.J., Huang, E.J., Nusse, R., et al. (2011). Axin2 as regulatory and therapeutic target in newborn brain injury and remyelination. Nat. Neurosci. *14*, 1009–1016. https://doi.org/10.1038/nn.2855.

51. Genoud, S., Lappe-Siefke, C., Goebbels, S., Radtke, F., Aguet, M., Scherer, S.S., Suter, U., Nave, K.-A., and Mantei, N. (2002). Notch1 control of oligodendrocyte differentiation in the spinal cord. J. Cell Biol. *158*, 709–718. https://doi.org/10.1083/jcb.200202002.

52. Tripathi, R.B., Rivers, L.E., Young, K.M., Jamen, F., and Richardson, W.D. (2010). NG2 glia generate new oligodendrocytes but few astrocytes in a murine experimental autoimmune encephalomyelitis model of demyelinating disease. J. Neurosci. *30*, 16383–16390. https://doi.org/10.1523/JNEUROSCI.3411-10.2010.

53. Zawadzka, M., Rivers, L.E., Fancy, S.P.J., Zhao, C., Tripathi, R., Jamen, F., Young, K., Goncharevich, A., Pohl, H., Rizzi, M., et al. (2010). CNS-resident glial progenitor/stem cells produce Schwann cells as well as oligodendrocytes during repair of CNS demyelination. Cell Stem Cell *6*, 578–590. https://doi.org/10.1016/j.stem.2010.04.002.

54. Wang, F., Yang, Y.-J., Yang, N., Chen, X.-J., Huang, N.-X., Zhang, J., Wu, Y., Liu, Z., Gao, X., Li, T., et al. (2018). Enhancing oligodendrocyte myelination rescues synaptic loss and improves functional recovery after chronic hypoxia. Neuron *99*, 689–701.e5. https://doi.org/10.1016/j.neuron.2018.07.017.

55. Dugas, J.C., Cuellar, T.L., Scholze, A., Ason, B., Ibrahim, A., Emery, B., Zamanian, J.L., Foo, L.C., McManus, M.T., and Barres, B.A. (2010). Dicer1 and miR-219 are required for normal oligodendrocyte differentiation and myelination. Neuron *65*, 597–611. https://doi.org/10.1016/j.neuron.2010.01.027.

56. Zhao, X., He, X., Han, X., Yu, Y., Ye, F., Chen, Y., Hoang, T., Xu, X., Mi, Q.-S., Xin, M., et al. (2010). MicroRNA-mediated control of oligodendrocyte differentiation. Neuron *65*, 612–626. https://doi.org/10.1016/j.neuron.2010.02.018.

57. Rutishauser, U., Ross, I.B., Mamelak, A.N., and Schuman, E.M. (2010). Role of the blood-brain barrier in the formation of brain metastases. Nature *464*, 903–907. https://doi.org/10.1038/nature08860.

58. Tamura, M., Spellman, T.J., Rosen, A.M., Gogos, J.A., and Gordon, J.A. (2017). Hippocampal-prefrontal theta-gamma coupling during performance of a spatial working memory task. Nat. Commun. *8*, 2182. https://doi.org/10.1038/s41467-017-02108-9.

59. Chang, K.J., Redmond, S.A., and Chan, J.R. (2016). Review Remodeling myelination : implications for mechanisms of neural plasticity. Nat. Neurosci. *19*, 190–197. https://doi.org/10.1038/nn.4200.

60. Pajevic, S., Basser, P.J., and Fields, R.D. (2014). Role of myelin plasticity in oscillations and synchrony of neuronal activity. Neuroscience *276*, 135–147. https://doi.org/10.1016/j.neuroscience.2013.11.007.

61. Cao, B., Wang, J., Zhang, X., Yang, X., Poon, D.C.H., Jelfs, B., Chan, R.H.M., Wu, J.C.Y., and Li, Y. (2016). Impairment of decision making and disruption of synchrony between basolateral amygdala and anterior cingulate cortex in the maternally separated rat. Neurobiol. Learn. Mem. *136*, 74–85. https://doi.org/10.1016/j.nlm.2016.09.015.

62. Plemel, J.R., Michaels, N.J., Weishaupt, N., Caprariello, A.V., Keough, M.B., Rogers, J.A., Yukseloglu, A., Lim, J., Patel, V.V., Rawji, K.S.,

et al. (2018). Mechanisms of lysophosphatidylcholine-induced demyelination: a primary lipid disrupting myelinopathy. Glia *66*, 327–347. https://doi.org/10.1002/glia.23245.

63. Deshmukh, V.A., Tardif, V., Lyssiotis, C.A., Green, C.C., Kerman, B., Kim, H.J., Padmanabhan, K., Swoboda, J.G., Ahmad, I., Kondo, T., et al. (2013). A regenerative approach to the treatment of multiple sclerosis. Nature *502*, 327–332. https://doi.org/10.1038/nature12647.

64. Li, Z., He, Y., Fan, S., and Sun, B. (2015). Clemastine rescues behavioral changes and enhances remyelination in the cuprizone mouse model of demyelination. Neurosci. Bull. *31*, 617–625. https://doi.org/10.1007/s12264-015-1555-3.

65. Liu, J., Dupree, J.L., Gacias, M., Frawley, R., Sikder, T., Naik, P., Casaccia, P., Liu, J., Dupree, J.L., Gacias, M., et al. (2016). Clemastine enhances myelination in the prefrontal cortex and rescues behavioral changes in socially isolated mice. J. Neurosci. *36*, 957–962. https://doi.org/10.1523/JNEUROSCI.3608-15.2016.

66. Pan, S., Mayoral, S.R., Choi, H.S., Chan, J.R., and Kheirbek, M.A. (2020). Preservation of a remote fear memory requires new myelin formation. Nat. Neurosci. *23*, 487–499. https://doi.org/10.1038/s41593-019-0582-1.

67. Giaume, C., Koulakoff, A., Roux, L., Holcman, D., and Rouach, N. (2010). Astroglial networks: a step further in neuroglial and gliovascular interactions. Nat. Rev. Neurosci. *11*, 87–99. https://doi.org/10.1038/nrn2757.

68. Araque, A., Carmignoto, G., Haydon, P.G., Oliet, S.H.R., Robitaille, R., and Volterra, A. (2014). Gliotransmitters travel in time and space. Neuron *81*, 728–739. https://doi.org/10.1016/j.neuron.2014.02.007.

69. Verkhratsky, A., and Nedergaard, M. (2018). Physiology of astroglia. Physiol. Rev. *98*, 239–389. https://doi.org/10.1152/physrev.00042.2016.

70. Demerens, C., Stankoff, B., Logak, M., Anglade, P., Allinquant, B., Couraud, F., Zalc, B., and Lubetzki, C. (1996). Induction of myelination in the central nervous system by electrical activity. Proc. Natl. Acad. Sci. USA *93*, 9887–9892. https://doi.org/10.1073/pnas.93.18.9887.

71. Kol, A., Adamsky, A., Groysman, M., Kreisel, T., London, M., and Goshen, I. (2020). Astrocytes contribute to remote memory formation by modulating hippocampal–cortical communication during learning. Nat. Neurosci. *23*, 1229–1239. https://doi.org/10.1038/s41593-020-0679-6.

72. Rinholm, J.E., Hamilton, N.B., Kessaris, N., Richardson, W.D., Bergersen, L.H., and Attwell, D. (2011). Regulation of oligodendrocyte development and myelination by glucose and lactate. J. Neurosci. *31*, 538–548. https://doi.org/10.1523/JNEUROSCI.3516-10.2011.

73. Lezmy, J., Arancibia-Cárcamo, I.L., Quintela-López, T., Sherman, D.L., Brophy, P.J., and Attwell, D. (2021). Astrocyte Ca2+-evoked ATP release regulates myelinated axon excitability and conduction speed. Science *374*, eabh2858. https://doi.org/10.1126/science.abh2858.

74. Ng, Q.X., Soh, A.Y.S., Loke, W., Lim, D.Y., and Yeo, W.-S. (2018). The role of inflammation in irritable bowel syndrome (IBS). J. Inflamm. Res. *11*, 345–349. https://doi.org/10.2147/JIR.S174982.

75. Lei, Z., Xie, L., Li, C.H., Lam, Y.Y., Ramkrishnan, A.S., Fu, Z., et al. (2022). Chemogenetic activation of astrocytes in the basolateral amygdala contributes to fear memory formation by modulating the amygdala–prefrontal cortex communication. Int. J. Mol. Sci. *23*, 6092. https://doi.org/10.3390/ijms23116092.

76. Iqbal, Z., Liu, S., Lei, Z., Ramkrishnan, A.S., Akter, M., and Li, Y. (2022). Astrocyte L-Lactate signaling in the ACC regulates visceral pain aversive memory in rats. Cells *12*, *26*. https://doi.org/10.3390/cells12010026.

STAR★METHODS

KEY RESOURCES TABLE

REAGENT or RESOURCE	SOURCE	IDENTIFIER
Antibodies		
Rabbit Anti-Myelin Basic Protein	Abcam	Cat# ab40390, RRID:AB_1141521
Mouse Anti-Neurofilament (NFL)	Abcam	Cat# ab7794; AB_306083
Mouse Anti-NG2 antibody	Abcam	Cat# ab50009, RRID:AB_881569
Mouse Anti-APC to CC1	Abcam	Cat# ab9610; RRID:AB_443473
Rabbit anti-Olig2	Millipore	Cat# ab9610; RRID:AB_570666
Rabbit anti-GFAP	Abcam	Cat# ab7260; RRID:AB_305808
Mouse anti-GFAP	Abcam	Cat# ab279290;
Rabbit amti-S100 β	Abcam	Cat# ab41548; RRID:AB_956280
Mouse anti-CD68	Abcam	Cat# ab31630; AB_1141557
Mouse anti-IL1β	Abcam	Cat# ab9722; RRID:AB_308765
Chicken anti-mCherry	Abcam	Cat# ab205402; RRID:AB_2722769
Rabbit anti-cFos	Abcam	Cat# ab208942; RRID:AB_2747772
Mouse anti-NeuN	Millipore	Cat# MAB377; RRID:AB_2298772
Rabbit Anti-MRF	Abcam	Cat# ab85464
Mouse anti-Beta actin	Immunoway	Cat# YM3628; AB_2629465
Rabbit anti-alfa tubulin	Sigma	Cat# T6074; RRID:AB_477582
Goat pAB to anti-Rabbit Alexa Fluor 488	Invitrogen	Cat# A11034; RRID:AB_2576217
Goat pAB to anti-Mouse Alexa Fluor 488	Invitrogen	Cat# A11029; RRID:AB_138404
Goat pAB to anti-Rabbit Alexa Fluor 594	Invitrogen	Cat# A1037; A11037; RRID:AB_2534095
Goat pAB to anti-Mouse Alexa Fluor 594	Invitrogen	Cat# A11032; RRID:AB_2534091
Goat pAB to anti-Rabbit Alexa Fluor 647	Abcam	Cat# ab150075; RRID:AB_2752244
Goat pAB to anti-Mouse Alexa Fluor 647	Invitrogen	Cat# A32728; RRID:AB_2633277
Anti-Mouse IgG (H + L) HRP	Invitrogen	Cat# 626520; RRID:AB_88369
Anti-Rabbit IgG (H + L) HRP	Invitrogen	Cat# 31466; RRID:AB_10960844
Goat pAB to Chk Alexa Fluor 594	Abcam	Cat# ab150172
Bacterial and virus strains		
AAV8-GFAP-hM3D(Gq)-mCherry	Vigene Biosciences, China	N/A
Chemicals, peptides, and recombinant proteins		
5-ethynyl-2′-deoxyuridine (EdU)	Invitrogen	Cat# A10044
Click IT EdU Alexa Fluor 555 Imaging Kit	Invitrogen	Cat# C10338
Lysophosphatidylcholine	USP	Cat# 1372050
Clozapine N-Oxide (CNO)	MCE, China	Cat# HY-17366A
Clemastine	Cayman Chemicals	Cat# 14637
Experimental models: Organisms/strains		
Sprague Dawley male rats	Chinese University of Hong Kong (CUHK), Hong Kong	RRID:RGD_10395233
Software and algorithms		
GraphPad Prism v7.0	GraphPad, CA, USA	RRID:SCR_002798
MATLAB	MathWorks, USA	RRID:SCR_001622
SPSS 24.0	Chicago, IL, USA	RRID: SCR_019096

(*Continued on next page*)

Continued

REAGENT or RESOURCE	SOURCE	IDENTIFIER
NeuroExplorer 5 software	Nex Technologies, Littleton, MA	N/A
OmniPlex® D system, Plexon	Plexon, Dallas, TX	N/A
Imetronic operant chamber and polyvalent data processing software	Imetronic, Pessac, France	N/A
Other		
16-channel polyimide-insulated platinum/iridium micro-wire electrode	Clunbury Scientific, MI, USA	N/A
Hamilton microsyringe	RWD, China	N/A
Microsyringe Pump	World Precision Instruments, USA	N/A

RESOURCE AVAILABILITY

Lead contact

Further information and requests for resources and reagents should be directed to and will be fulfilled by the Corresponding Author/Lead Contact, Dr. Ying Li (yingli@cityu.edu.hk).

Materials availability

This study did not generate any new unique reagents.

Data and code availability

All data produced in this study are included in the published article and its supplemental information, or are available from the lead contact upon request.

This paper does not report original code.

Any additional information required to reanalyze the data reported in this paper is available from the lead contact upon request.

EXPERIMENTAL MODEL AND SUBJECT DETAILS

Animals and ethical consideration

All experiments were conducted with healthy, experimentally naive adult male Sprague-Dawley (SD) rats (250–350 g). The animals were housed in home cages on a 12:12 h light-dark cycle (lights on 7:30a.m.) with food and water provided *ad libitum*. For all experiments rats were randomly selected to experimental groups. All the experimental procedures were conducted according to the guidelines laid down by the NIH in the US with the approval of the Committee on the Use and Care of Animals at City University of Hong Kong, and the authorization license for performing all the tests issue by the Department of Health of Hong Kong (Reference: Rev(19-177) in DH/HT&A/8/2/5 Pt.1; (21-53) in DH/HT&A/8/2/5 Pt.5; (21-56) in DH/HT&A/8/2/5 Pt.5). Specific details of rats in each experiment are provided below.

Visceral hypersensitivity (VH) rat model

For the initial behavioral task, the subjects were 58 male SD rats collected from Laboratory Animal Service Center of Chinese University of Hong Kong (CUHK). For immunohistochemistry and TEM, subjects were 18 male SD rats collected from CUHK.

Focal demyelination

Subjects were 49 male SD rats obtained from Laboratory Animal Service Center of Chinese University of Hong Kong (CUHK).

Drug (clemastine) induced remyelination

Subjects were 31 male SD rats obtained from Laboratory Animal Service Center of Chinese University of Hong Kong (CUHK). For VMR studies, 6 rats were used in a different cohort.

Chemogenetic activation of astrocytic Gq pathway

The subjects were 60 male SD rats obtained from Laboratory Animal Service Center of Chinese University of Hong Kong (CUHK).

In vivo electrophysiology recordings

The subjects were 10 SD male rats obtained from Laboratory Animal Service Center of Chinese University of Hong Kong (CUHK).

METHOD DETAILS

Development of VH animal model

The detailed procedures have been described in our previous publications.[9,12–14] Rats adapted to their environments for at least 3 days before VH was induced by intraperitoneal injection with 10 μg egg albumin (antigen) and 10 mg aluminum hydroxide (adjuvant) in 1 mL saline. From the third day to the fifth day after antigen injection, the rats were given a colonic perfusion with antigen solution (composed of 10 μg/mL egg albumin, 40 mM D-glucose) at 50 μL/min for 30 min, followed by 30 mm Hg colorectal anaphylaxis for 30 s repeated 5 times with 3-min intervals. Control rats were injected intraperitoneally with 1 mL saline and colorectally perfused saline for 30 min. Our previous studies showed allodynia and hyperalgesia and ACC hypersensitivity to colorectal distension can be observed up to 7 weeks after the initiation of colonic anaphylaxis.[9,12–14]

Surgery

For all the surgeries, rats were anesthetized with pentobarbital and their head were placed in a stereotactic frame. The fur was removed, and skulls was exposed, and a small craniotomy was performed bilaterally into the ACC region by using following coordinates: AP 2.2- 3.8 mm, ML 0.5-1 mm; and DV 1.5-3.5 mm from bregma.

Viral injection

For viral injection, after craniotomy (0.5-0.8 mm small hole), a volume of 0.4 μL per hemisphere AAV virus solution (diluted 1:10) containing GFAP-hM3D(Gq)-mCherry vector (Vigene, China) was injected bilaterally into the ACC region, at a rate of 0.5 μL/min with a 10 μL Hamilton microsyringe (Hamilton, NV, USA), controlled by a microsyringe pump (World Precision Instruments, FL, USA) and its controller (WPI). After the injection, the needle was kept in the place for an additional 5 min to facilitate the diffusion of the virus after which it was slowly withdrawn. Rats were kept for three-four weeks after virus injection to allow genes expression.

Focal demyelination

Anesthetized rats were placed into a stereotactic apparatus using flat skull position. Lysolecithin (LPC, EMD Chemicals) was dissolved in artificial cerebrospinal fluid (aCSF), 2 μL 1% LPC was administered bilaterally into the ACC (the coordinates are 2.4 mm anterior to bregma; 0.8 mm lateral; and 2.0 mm dorsal to ventral) using a Hamilton syringe (31-gauge Hamilton needle) connected with microinjector for a period of 5 min (and aCSF as a control). The ACC was defined as the cingulate cortex, area 2 and prelimbic cortex together with the overlying cingulate cortex, area 1,[9] which is a major cortical area of the limbic system, integrating emotion and cognition.

Drug Administration

For remyelination studies, rats were treated with Clemastine (dissolved in DMSO at 10 mg/mL before further dilution in double distilled water, 10 mg/kg body weight) daily through oral gavage for 2 weeks (7 days after VH induction) to promote remyelination in VH rats. Saline was used as a vehicle.

For chemogenetic studies, CNO was dissolve in DMSO and then diluted in normal saline to get final concentration of 0.5%. Control solution was also consisting of normal saline containing 0.5% DMSO. CNO was administered intraperitoneally at the rate of 3 mg/kg, 30 min before the RGT. This dose did not cause any behavioral signs of seizure tested by open field.

Rat gambling task (RGT)

The RGT is a task that is used to test the decision-making behavior in rats by introducing conflict between immediate and long-term gratification based on successive choice between food rewards of different values and probabilities.[18,19] In brief, food was restricted before the training to maintain 80% of free feeding body weight for 3 days following 1-day fasting. During the training sessions which lasted for 7-10 days to learn the association between nose-pokes and food rewards in the polyvalent conditioning chamber. The operant chambers (28 × 30 × 34 cm, Imetronic, Pessac, France) consisted of four nosepoke apertures on the front and one food dispenser on the opposite wall for releasing food pellets as rewards. The rats were food restricted to 80% of their free feeding weight during the entire RGT procedure.

During training, each rat was placed in the chamber for 40 min each day, to gradually understand the association between the nose-poke action and the release of a food pellet. The entire test procedure lasted 60 min and was performed on the day after training completion. Rats were free to choose between the four nose pokes (A–D) as they were during the training phase; however, each choice was associated with different food reward and different likelihood of a timeout-penalty. Nose poke A or B led to immediate delivery of two pellets but had a 50% likelihood to trigger a 222 s penalty time-out and a 25% likelihood for a 444 s time-out, during which no pellets could be obtained. Nose pokes C or D were associated with smaller immediate rewards (one pellet), but also smaller penalties (25% likelihood for a 12s time-out, or 50% likelihood for a 6 s time-out). Therefore, in the long run the maximum benefit of collecting food reward associated with C and D was five times than that of A and B. Hence, the nosepokes C and D were more advantageous for the rats to collect as many food pellets as possible. The good decision-making rats learned the uncertain, risky choices in nosepoke A and B within few trials and therefore avoided choosing those nosepokes and progressively favored non-risky, advantageous choices in nosepoke C and D during the latter part of the task, whereas poor decision-making rats chose nosepoke A and B for immediate gratification, and the rats failed to learn these outcomes chose the options randomly. The percentage of advantageous choices chosen in the last 20 min was used as a criterion to distinguish the good (>70% advantageous choices), poor (<30% preference) decision-makers and undecided (30%–70% preference). If a rat showed preference for a specific nosepoke throughout the training and test, it was excluded from further analysis. The percentage of advantageous choices [(C + D)/(A + B + C + D)×100%] during the last 20 min and the total food rewards obtained across the test were used to identify the decision-making behavior of the rats.

Immunohistochemistry

To identify the effect of chronic visceral hypersensitivity on ACC and corpus callosum myelination, rats were sacrificed 7 days after VH induction. Rats' brains were post fixed in 4% PFA overnight at 4°C. Tissue were cryoprotected in 10%, 20%, 30% (w/v) sucrose before freezing in OCT. ACC tissue sections [2.2 to 3.8 mm coordinates from the bregma (cc, corpus callosum; cingulate cortex, area 1; cingulate cortex, area 2; prelimbic cortex)] were collected. 20-30 μm slices of the brain were collected and processed as floating slices. Primary antibodies, rabbit anti-MBP (1:500), labels the myelinated fibers, Mouse anti-NG2 (1:500), Mouse anti-CC1 (1:500 dilution), Rabbit anti IBA1 (1:500), Mouse anti-CD68 (1:500), Mouse anti-IL1 beta (1:500), Rabbit anti-IL6 (1:500), Rabbit antiGFAP (1:500, Sigma-Aldrich), Mouse anti S100β (1:1000, Abcam), Mouse antiNeuN (1:1000, Millipore), Chicken anti m-Cherry (1:1000, Abcam) diluted in blocking solution (0.1% [v/v] Triton X-100 and 10% goat serum in 0.01 M PBS) and was applied to slices overnight at 4°C. Then slices were washed and incubated for 2 h with respective secondary antibodies. Finally, slices were mounted on slides and imaged by using an inverted laser scanning confocal microscope (FV1000; Olympus).

EdU labeling

To estimate the overall OPC and OLs proliferation in response to chronic visceral hypersensitivity, 5 ethynyl-2′-deoxyuridine (EdU) was administered i.p at dose of 25 mg/kg immediately after last date of colorectal anaphylaxis, and 2.5 - 5 mg/L from day 7 to day 14 after VH induction on separated groups. The rats were euthanized on day 4 and day 15 and brain samples containing ACC were sectioned and co-labelled with monoclonal anti-CC1 and anti-NG2 antibodies along with EdU using the Alexa Fluor 555 Click-iT detection kit (Invitrogen) (Hasan et al., 2019).

Immunohistochemistry to determine the biomarker for reactive astrogliosis and neuroinflammation

Inflammation may play a pathogenic role in IBS. Studies have emphasized the occurrence of mucosal inflammation at the microscopic and molecular level in IBS and the proliferation of enteroendocrine cells, mast cells and other inflammatory cells, causing neuroinflammation through the gut-brain axis.[74] Therefore, we are curious to see whether neuroinflammatory cells and astrocytes are also reactive in our established chronic visceral hypersensitive model that can mimic the IBS. To characterized this, we performed immunohistochemistry and western blot to determine the relative expression of reactive microglial cells ($CD68^+$ and $IBA1^+$ cells, biomarkers for reactive microglial), inflammatory cytokines IL1 beta and IL6 (biomarkers for inflammatory cytolines) and astrogliosis marker Rabbit antiGFAP (1:500, Sigma-Aldrich), Mouse anti S100β (1:1000, Abcam) in the ACC of VH and control rats.

Confocal imaging and processing

Slices were mounted on slides and imaged by using an inverted laser scanning confocal microscope (FV1000; Olympus). A total of 3–5 sections were examined per rat, and 3-5 rats were analyzed per group. Confocal images represent projected stacks of 10 images collected at 1-2 μm steps. The MBP^+ intensity was measured up to 1000 μm from the plial surface (midline) covering layers I-VI in the ACC region. The myelin MBP^+ intensity is calculated using ImageJ. The MBP+ intensity was normalized with the control samples. The number of $NG2^+$, $CC1^+$, EdU+ co-labeling cells, $CD68^+$, $IBA1^+$, $IL1^+$ and $IL6^+$ cells were also calculated in the field of view containing layers I-VI.

Protein extraction and western blot analysis

Western blot analysis was conducted from brain lysate collected from ACC, using the protocol from our previously published paper.[18,19] The following commercial primary and secondary antibodies were used at the indicated dilutions: anti-rabbit MBP (1:5000), anti-rabbit MYRF (1:250), anti-mouse IL1 (1:500), anti-rabbit IL6 (1:500) and anti-mouse β-actin (1:5000, Immuno Way), anti-mouse HRP (Invitrogen) and anti-rabbit HRP (Invitrogen).

TEM microscopy

TEM microscopy was conducted by following our previous established method (Hasan et al., 2019). Briefly, rats were perfused with 0.1 M PB followed by 2% glutaraldehyde/4% PFAin sodium cacodylate buffer. A block of approximately 1 × 1 × 2mm3 from the right ACC was dissected out and then post fixed with the primary fixative, then contrasted with 1% osmium tetroxide (v/v) in PBS. Tissues were dehydrated in an ethanol graded from 50 to 100% and embedded in Epon. Ultra-thin Slices (80 nm) was cut and stained with 2% uranyl acetate (v/v) and Reynold's lead citrate and analyzed imaged with Gatan Orius digital camera. G-ratio is calculated by dividing the diameter of an axon by that of total fiber diameter (axon + myelin sheath) from 150-180 fibers in ACC.

Multiple-channel electrophysiology recording in ACC and BLA

The detailed procedures have been described in our previous publications (Cao et al., 2016a; Hasan et al., 2019; Wang et al., 2017). Two 16-channel polyimide-insulated platinum/iridium micro-wire electrode arrays (4 × 4, electrode diameter = 25 μm; 250 μm spacing between each, impedance = 20–50 kΩ; Clunbury Scientific, MI, USA) were inserted into the ACC and BLA one week after VH induction (ACC: anterior-posterior (AP) = 3.0-3.3, Medial-lateral (ML) = 0.6-1.0, dorsal-ventral (DV) = 2.8-3.5 mm from dura) and the ipsilateral BLA (AP -3.3 to - 3.6, ML 5.0-5.3, depth 6.5-7.5 mm). One wire from each array was wrapped around one of the bones mounting screws to ground. LFPs and spike firing were recorded with an electrophysiological data acquisition system (OmniPlex D system, Plexon, Dallas, TX). LFPs were amplified (×20,000), band-pass filtered (0.05 - 200 Hz, 4-pole Bessel) and sampled at 1 kHz. Spikes were identified when a minimum waveform reached an amplitude threshold of 4.5 standard deviations higher than the noise amplitude, and were filtered (300 - 5,000 Hz, 4-pole Bessel) and sampled at 40 kHz. Signals from the ACC and BLA were recorded simultaneously during 60s spontaneous activity.

Rats were allowed to recover from electrode implantation surgery for 1 week. After recovery, Clemastine treatment is started in VH rats, and the signals were recorded on days 7 and 14 after start of Clemastine treatment i.e. Third week and fourth week after VH induction. Similar recordings are performed in saline

treated VH rats and control rats after 7 days i.e third week after VH induction and control preparation, respectively.

Dataacquisition and spike sorting

After 6-8 days recovery, the local field potential (LFP) and spike activities were recorded using a multiple-channel neural data acquisition system (Omniplex D, Plexon). Spike signals were amplified (×1000), band-pass filtered (0.3-5 kHz, 4-pole Bessel) and sampled at 40 kHz. LFPs were amplified (×1000), band-pass filtered (0.05-200 Hz, 4-pole Bessel) and sampled at 1 kHz. Two minutes' data was recorded for each rat in a quiet waking state in home cages. Single unit spike sorting was detected by thresholding and sorted by offline using Offline Spike Sorter software (Version 4, Plexon Inc.), as described in our recent publications.[18,19]

Spike-field coherence (SFC)

Temporal coding is important regulator in memory and perception (Cao et al., 2016a; Hasan et al., 2019; Wang et al., 2017). To measure the strength of synchrony between spike timing and phase of field potential oscillations, we quantified the SFC as described previously.[18,19] To compute the SFC across the ACC and BLA, the spikes recorded in the ACC and the averaged LFP from the BLA were used in the analyses. To ensure the validity of the statistical results, only neurons which had at least 50 spikes during the period analyzed were used for SFC analysis.

Phase-locking of single neuron spikes to the theta oscillation

To study the angular distribution of ACC spikes in relation to the BLA theta oscillation and clarify the strength of phase-locking, we plotted the phase distribution and analyzed Rayleigh test using custom written MATLAB scripts as described previously.[18,19] To ensure the validity of the statistical results, only neurons with at least 50 spikes during the period analyzed were used for phase-locking estimation.

Cross-correlation analyses

To identify the relationship of the time course of coordinated activity between ACC and BLA, the synchronized theta activities (4-10 Hz) between ACC and BLA were evaluated by computing cross-correlograms using NeuroExplorer 5 software (Nex Technologies, Littleton, MA), as described previously.[18,19] Theta-filtered LFPs from the ACC and BLA were aligned, and the LFP in the ACC was chosen as the reference.

Exclusion of animals and neurons

In RGT studies, several rats were excluded for analysis due to inactive and failure to reach the criterion of training for the whole period (1 control rat, 1 VH + Cle rat, 1 VH + CNO, 2 VH + Sal rats and 2 Con + CNO rats). Several rats were excluded from this study due to either misplacement of electrode (n = 1) or virus expression (n = 3).

QUANTIFICATION AND STATISTICAL ANALYSIS

Data are expressed as mean ± SEM (SE of mean) unless otherwise mentioned in figure legends. Statistical significance analyzed with GraphPad Prism v7.0 (GraphPad, CA) or SPSS 24.0 (Chicago, IL, USA). When the data met the assumptions of parametric statistical tests, results were analyzed by Student's *t* test or two-way ANOVA, followed by posthoc tests, as applicable. Subjects were excluded from analysis when they deviated by more than two standard deviations from the mean. The data showing the proportion of decision-makers is presented in ordinal coordinates with a nonnormal distribution; therefore, a Mann-Whitney U test was performed to assess significance. The electrophysiological data was analyzed with two-way ANOVA analysis followed by Bonferroni's post-hoc tests for multiple comparisons. The data with normal distribution with mean and variance of two groups are analyzed with 2-tailed unpaired t-test. A value of $p < 0.05$ was considered statistically significant for all comparisons, except for Rayleigh's test where $p < 0.0023$ (0.05/22 frequencies tested) was considered significant phase locking.